Theory Manual for the Copper Corrosion Model for Uniform Corrosion in Sedimentary Rock CCM-UC.1.1

NWMO TR-2008-07 **April 2008**

Fraser King

Integrity Corrosion Consulting Limited

nwmo

NUCLEAR WASTE MANAGEMENT ORGANIZATION

SOCIÉTÉ DE GESTION DES DÉCHETS NUCLÉAIRES

Nuclear Waste Management Organization
22 St. Clair Avenue East, 6th Floor
Toronto, Ontario
M4T 2S3
Canada

Tel: 416-934-9814
Web: www.nwmo.ca

Theory Manual for the Copper Corrosion Model for Uniform Corrosion in Sedimentary Rock CCM-UC.1.1

NWMO TR-2008-07

April 2008

Fraser King
Integrity Corrosion Consulting Limited

ABSTRACT

Title: **Theory Manual for the Copper Corrosion Model for Uniform Corrosion in Sedimentary Rock CCM-UC.1.1**
Report No.: **NWMO TR-2008-07**
Author(s): Fraser King
Company: Integrity Corrosion Consulting Limited
Date: April 2008

Abstract
A mechanistically based model for the uniform corrosion of copper used fuel containers in a deep geological repository in sedimentary deposits is described. The model is termed the Copper Corrosion Model for Uniform Corrosion (CCM-UC). The mechanism accounts for all of the important processes involved in the corrosion of copper in porous media in contact with O_2-containing chloride solutions, including: interfacial electrochemical reactions, precipitation/dissolution, adsorption/desorption, redox, and mass-transport processes. These processes have been selected based on the results of an extensive experimental program with copper (Cu) materials.

These processes are expressed mathematically in the form of a series of ten coupled, one-dimensional reaction-diffusion equations, one for each of the chemical species included in the model, namely: gaseous and dissolved O_2, dissolved $CuCl_2^-$, precipitated Cu_2O, dissolved and adsorbed Cu^{2+}, precipitated $CuCl_2 \cdot 3Cu(OH)_2$, Cl^-, and dissolved and precipitated Fe(II). In addition, a heat-conduction equation is included to account for the spatial and temporal variation of temperature within the repository.

From a corrosion viewpoint, the two characteristics of typical deep sedimentary formations that distinguish them from a crystalline host rock are the higher salinity groundwater and the lower hydraulic conductivity. The higher groundwater salinity, especially the higher chloride concentration, will (i) promote uniform corrosion over localized corrosion or stress corrosion cracking, (ii) effect the speciation and stability of Cu(I) species, and (iii) inhibit microbial activity. The lower hydraulic conductivity will result in an extended unsaturated period in the deep geological repository which will have the following effects: (i) a period of no aqueous corrosion, (ii) faster diffusion of O_2 and slower diffusion of dissolved species, and (iii) restricted microbial activity.

The mathematical treatment of the various processes and their dependence on the repository design and environmental factors such as temperature, redox conditions, and the degree of saturation are described. The model incorporates an electrochemical mixed-potential model which allows the prediction of the corrosion potential and the corrosion rate. Finally, the finite-difference technique used to solve the reaction-diffusion equations is also described in some detail.

TABLE OF CONTENTS

LIST OF TABLES

Page

LIST OF FIGURES

Page

1. INTRODUCTION

The Nuclear Waste Management Organization (NWMO) is conducting a research and development (R&D) program to support implementation of Adaptive Phase Management for long-term management of Canada's used nuclear fuel (NWMO 2005). The NWMO's R&D program includes advancing the technologies associated with a deep geological repository (DGR) for used fuel in a suitable geological formation, such as crystalline rock or sedimentary deposits. Any such repository would be based on a multi-barrier design, comprising a number of natural and engineered barriers (Russell and Simmons 2003). One of the engineered barriers would be a long-lived metallic used-fuel container (UFC) designed to provide long-term containment and isolation of used fuel for a considerable length of time in a DGR.

Two materials are being considered as corrosion barriers for the UFC. Copper (Cu) has long been considered in Canada, and oxygen-free, phosphorus-doped (OFP) copper is the reference container material for a DGR in crystalline rock (Gierszewski et al. 2004, Maak 1999). More recently, carbon steel has been considered as an alternative to copper for a repository in sedimentary deposits (King 2005a,b; 2007). Copper is also considered a suitable corrosion barrier material for UFC for a repository in sedimentary deposits.

Prediction of the performance of a copper UFC in a DGR requires the development of models to predict the long-term corrosion behaviour in the repository environment. A series of models has been developed for predicting the corrosion performance of copper UFC and are denoted by the general designation Copper Corrosion Model (CCM). Versions of the CCM have been developed to predict the uniform corrosion behaviour in crystalline rock (King and Kolar 1995, 1996, 1997a,b, 2000, 2006a; Kolar and King 1996), microbiologically influenced corrosion (MIC) (King and Kolar 2006b; King et al. 2002a, 2003, 2004), and stress corrosion cracking (SCC) (King and Kolar 2004, 2005).

Following its initial development in 1995 the copper corrosion model for uniform corrosion (CCM-UC) has undergone a number of improvements. The latest version of the model, CCM-UC.1.1, was used to predict the evolution of the corrosion behaviour and of the redox conditions for various large-scale experiments and a specific repository design in crystalline rock (King and Kolar 2006a). This version of the model includes improved treatment of the effects of the unsaturated period on the mass transport of species and on the interfacial electrochemical reactions occurring on the container surface.

The NWMO have recently begun to investigate the properties of sedimentary deposits as a possible host formation for a DGR (Mazurek 2004). Old, stable, horizontally bedded shale and limestone deposits of Ordovician age can be found throughout southern Ontario and elsewhere in Canada. Although detailed site investigation is still required, it is apparent that the environmental conditions for a DGR constructed in the shale or limestone sedimentary deposits would differ from those in crystalline rock in a number of ways. For example, deep groundwaters in the Ordovician sedimentary deposits are more saline than those found at a similar depth in the crystalline rock of the Canadian Shield. Salinities of several hundred thousand mg/L are found at a typical repository depth of 500-600 m, equivalent to a chloride ion concentration of several mol·dm^{-3} (King 2005a, McMurray 2004). Chloride ions play a significant role in the corrosion of Cu because of the complexation of Cu(I) in the form of cuprous-chloro complex ions. The second significant difference between sedimentary deposits and crystalline rock is the lower hydraulic conductivity of the former. Again, although site-

specific data are not available, the hydraulic conductivity of deep Queenston shale and Cobourg limestone (previously known as Lindsay limestone) formations are of the order of 10^{-12} m·s^{-1} (Golder 2003, King 2005a), compared with a typical value of 10^{-10}-10^{-9} m·s^{-1} at repository depth in the Canadian Shield (McMurray et al. 2003). As a consequence, saturation of the repository will be slower in sedimentary formations leading to a longer period of corrosion under unsaturated conditions.

This report describes a theory manual for the copper corrosion model for uniform corrosion of OFP copper. The report focuses on a DGR in sedimentary host rock, although many aspects of the model and the mechanism on which it is based would also apply to a repository in crystalline rock as well. From a mechanistic viewpoint, the version of the model described here is CCM-UC.1.1, as described by King and Kolar (2006a). This theory manual follows the same format as that previously used for the models for MIC (King et al. 2002a) and SCC (King and Kolar 2004). First, the scientific basis and the reaction scheme for the model are described, followed by a discussion of the underlying assumptions inherent in the model. Next, the mathematical aspects of the model are considered. The development of the reaction-diffusion equations, model geometry, and initial and boundary conditions is discussed in detail. Finally, the numerical methods used to solve the reaction-diffusion equations are described.

2. MECHANISM OF THE UNIFORM CORROSION OF COPPER UFC

2.1 CORROSION OF COPPER IN COMPACTED BENTONITE

The mechanism of the corrosion of copper in O_2-containing chloride solutions in porous media has been studied in detail (King et al. 2001, 2002b). The important aspects of this mechanism are summarized below, and are described in more detail by King and Kolar (2000) and King et al. (2001, 2002b).

2.1.1 Interfacial Electrochemical Reactions

The corrosion of copper UFC is an electrochemical process involving one anodic dissolution reaction coupled to one or more cathodic reduction reactions (King and Kolar 2000; King et al. 2001, 2002b). In Cl^- environments, dissolution occurs as Cu(I)-Cl^- complexes of the form $CuCl_2^-$, $CuCl_3^{2-}$, etc. Many authors have studied this reaction (Bacarella and Griess 1973, Bjorndahl and Nobe 1984, Bonfiglio et al. 1973, Braun and Nobe 1979, Crundwell 1992, Deslouis et al. 1988a,b, Dhar et al. 1985, Faita et al. 1975, Hurlen 1961a,b, Kato et al. 1980a,b, Kear et al. 2004, Lee and Nobe 1986, Lee et al. 1985, Moreau 1981a,b, Moreau et al. 1982, Smyrl 1985) and the consensus is that the reaction can be best described by the two-stage process

$$Cu + Cl^- = CuCl_{ADS} + e^- \quad (1)$$

$$CuCl_{ADS} + Cl^- = CuCl_2^- \quad (2)$$

The electrochemical rate expression for the overall process is

$$i_a = n_a F\left\{k_a [Cl^-]_0^2 \exp\left[\frac{F}{RT}(E - E_a^0)\right] - k_{bb}[CuCl_2^-]_0\right\} \quad (3)$$

where i_a is the anodic current density, n_a the number of electrons transferred, F is the Faraday constant, k_a is a combined rate constant equivalent to $k_{af}k_{bf}/k_{ab}$ (where k_{af} and k_{ab} are the forward and reverse electrochemical rate constants for Reaction (1) and k_{bf} is the forward rate constant for Reaction (2)), $[Cl^-]_0$ is the interfacial concentration of Cl^- ions (here, concentrations are used in place of the more strictly correct activities), R and T are the gas constant and absolute temperature, E is the electrochemical potential, E_a^0 is the standard potential for Reaction (1), k_{bb} is the reverse rate constant for reaction (2), and $[CuCl_2^-]_0$ is the interfacial concentration of $CuCl_2^-$.

Sulphate ions, which do not form strong complexes with Cu(I), are also present in deep sedimentary pore waters, albeit at lower concentrations than Cl^- ions (McMurray 2004, King 2005a). However, King and Tang (1998) have shown that Reaction (1) predominates, even in equimolar concentrations of Cl^- and SO_4^{2-}. Since Cl^- is the predominant anion in sedimentary pore waters, Cu will dissolve as Cu(I) only.

The anodic dissolution of copper is coupled to two cathodic reactions, the reduction of O_2 (King et al. 1995a,b; Vazquez et al. 1994a,b)

$$O_2 + 2H_2O + 4e^- \rightarrow 4OH^- \quad (4)$$

and the reduction of Cu(II) (Peters and Cruser 1965)

$$Cu^{2+} + 2Cl^- + e^- \rightarrow CuCl_2^- \quad (5)$$

The corresponding electrochemical rate expressions are

$$i_c = -n_c F k_c [O_2]_0 \exp\left[-\frac{\alpha_c F}{RT}(E - E_c^0)\right] \quad (6)$$

where i_c is the cathodic current density, n_c is the overall number of electrons transferred ($n_0 = 4$), k_c is the forward electrochemical rate constant for Reaction (4), $[O_2]_0$ is the interfacial concentration of O_2, and α_c and E_c^0 are the cathodic transfer coefficient and standard potential for Reaction (4), respectively, and

$$i_d = -n_d F k_d [Cu^{2+}]_0 \exp\left[-\frac{\alpha_d F}{RT}(E - E_d^0)\right] \quad (7)$$

where i_d is the cathodic current density for Reaction (5), n_d the number of electrons transferred ($n_d = 1$), $[Cu^{2+}]_0$ is the interfacial concentration of Cu^{2+} and k_d, α_d and E_d^0 are the standard electrochemical rate constant, cathodic transfer coefficient and standard potential of Reaction (5), respectively.

Under freely corroding conditions, as for the corrosion of a copper UFC, the rate of the anodic reaction is balanced by the sum of the rates of the two cathodic reactions

$$i_a = -(i_{c1} + i_{c2}) = i_{CORR} \quad (8)$$

with the rate equal to the corrosion current density i_{CORR}. This equality is the mathematical representation of the so-called mixed-potential theory of corrosion reactions. Generally, the equality represented by Equation (8) is valid at a unique electrochemical potential referred to as the corrosion potential E_{CORR}. These electrochemical expressions (Equations (3), (6), and (7)) are used in the CCM-UC as mathematical boundary conditions to solve the series of reaction–diffusion equations.

The validity of this treatment of the corrosion of copper in O_2-containing Cl^- solutions has been demonstrated by King et al. (1995c). Measurements of E_{CORR} were made over a range of Cl^- concentrations (0.1 mol·dm^{-3} to 1.0 mol·dm^{-3}), dissolved O_2 concentrations (approximately 10^{-7} mol·dm^{-3} to 2 x 10^{-4} mol·dm^{-3}), and mass transfer coefficients (10^{-6} cm·s^{-1} to 10^{-2} cm·s^{-1}) and then compared to predictions from a steady-state mixed-potential model based on Equations (3) and (6). Good agreement was found between measured and predicted E_{CORR}, and the steady-state model was able to predict the variation of E_{CORR} with each of the experimental parameters. This ability to be able to predict E_{CORR} over a wide range of experimental conditions provides confidence that the reactions selected to represent the interfacial reactions on the container surface are appropriate.

2.1.2 Redox Processes

In O_2-containing Cl^- solutions, Cu(II) species are formed from the homogeneous oxidation of Cu(I) by dissolved O_2 (Sharma and Millero 1988)

$$4Cu(I) + O_2 + 2H_2O \rightarrow 4Cu(II) + 4OH^- \quad (9)$$

The reaction is essentially irreversible, especially in environments that stabilize Cu(II), such as the complexant-containing solution used in the experimental studies (Sharma and Millero 1988) or the cation-exchanging Na-bentonite present in compacted buffer material. The reaction is first order with respect to both $[O_2]$ and [Cu(I)]. The rate constant increases with pH and temperature, but decreases with $[Cl^-]$ due to the stabilization of Cu(I) as $CuCl_2^-$ (Sharma and Millero 1988). These observations are consistent with the observed speciation of copper corrosion products in experiments performed under simulated repository conditions with varying $[O_2]$ and $[Cl^-]$ (King et al. 1992, 1997; Litke et al. 1992).

The rate expression for this reaction is

$$-\frac{d[CuCl_2^-]}{dt} = k_1[CuCl_2^-][O_2] \quad (10)$$

where k_1 is the second-order rate constant for the oxidation of $CuCl_2^-$ by O_2.

In solution, the half-life of Cu(I) in aerated 1 mol·dm^{-3} Cl^- (pH 7) at 25°C is of the order of 150 s (Sharma and Millero 1988). Thus, under aerated conditions at least, the rate of Cu(I) oxidation is fast compared to the expected transit time of $CuCl_2^-$ through the buffer material.

Oxygen is also expected to react with ferrous minerals in the repository (Johnson et al. 1994, 1996, King and Kolar 1997a, Kolar and King 1996). Ferrous minerals could be present in a number of forms in the repository. Preliminary geochemical investigations suggest that there

are pyrite impurities in crystalline rock (Spiessl et al. 2006) and it is anticipated that pyrite will also be potentially present in sedimentary rock. This host rock could be used as aggregate in some of the clay-based buffer and backfill sealing materials in the repository. Natural bentonites also contain Fe(II)-containing impurities, such as small quantities of Fe_3O_4 in the form of spherical particles (King 1991).

The homogeneous consumption of O_2 by Fe(II) can be considered to proceed via a number of steps. First, Fe(II) must dissolve from the mineral surface

$$\text{Fe(II) (s)} \rightarrow \text{Fe(II) (aq)} \tag{11}$$

(ferrous species are referred to generically as Fe(II) since the detailed speciation of dissolved ferrous species is not included in the model). Many minerals dissolve according to a "shrinking-core" model, in which an altered layer depleted in the element of interest precipitates as the mineral dissolves. The kinetics of such reactions are described by

$$\frac{d[\text{Fe(II)}]}{dt} = A_F[R_0 \exp(-\alpha_F t) + R_1] \tag{12}$$

where A_F is the area of exposed mineral per unit volume of buffer, backfill or rock, R_0 and R_1 are the initial and steady-state Fe(II) dissolution rate, and α_F determines the rate at which the steady-state dissolution rate is attained. A steady state is eventually established in which the dissolution rate of Fe(II) is governed by the dissolution rate of the least-soluble component of the mineral lattice. The values of α_F, R_0 and R_1 will vary from mineral to mineral.

Following dissolution, Fe(II) is rapidly oxidized in solution by O_2, according to

$$4\text{Fe(II)} + O_2 + 2H_2O \rightarrow 4\text{Fe(III)} + 4OH^- \tag{13}$$

followed by irreversible precipitation of $Fe(OH)_3$, at the pH of interest in natural waters. The kinetics of Reaction (13) are strongly pH-dependent (Stumm 1992), with (at pH > 5)

$$-\frac{d[\text{Fe(II)}]}{dt} = k[\text{Fe(II)}][OH^-]^2[O_2] \tag{14}$$

where the rate constant k_5 defined in the model is the term $k[OH^-]^2$.

At low $[O_2]$, the rate of Fe(II) oxidation (Equation (14)) may become smaller than the rate of Fe(II) dissolution (Equation (12)). Under those circumstances, Fe(II) will accumulate in the system and may ultimately precipitate (see below).

Dissolved Fe(II) may also react with Cu^{2+} via the overall reaction

$$Cu^{2+} + 2Cl^- + \text{Fe(II) (aq)} \rightarrow \text{Fe(III)} + CuCl_2^- \tag{15}$$

This reaction is assumed here to be first order with respect to both $[Cu^{2+}]$ and [Fe(II)]

$$-\frac{d[\text{Fe(II)}]}{dt} = -\frac{d[Cu^{2+}]}{dt} = k_6[Cu^{2+}][\text{Fe(II)}] \tag{16}$$

where k_6 is the corresponding second-order rate constant.

2.1.3 Precipitation and Dissolution Processes

Precipitated corrosion products are found on the surfaces of copper coupons exposed to compacted bentonite wetted with O_2-containing Cl^- solutions (King et al. 1992, 1997; Litke et al. 1992). Precipitation is most likely to occur at the copper/bentonite interface, as it is here that the concentration of dissolved Cu is highest. The predominant corrosion products observed experimentally were Cu_2O and basic cupric chloride ($CuCl_2 \cdot 3Cu(OH)_2$), as identified by X-ray diffraction. When exposed to natural environments, copper typically forms a duplex corrosion product layer, with an underlying layer of Cu_2O covered by a layer of a basic cupric salt, with the nature of the anion dependent upon the nature of the environment (King et al. 2001, 2002b).

The detailed mechanism by which the inner layer of Cu_2O forms is not completely understood, but may involve the dehydration of a $Cu(OH)_{ADS}$ intermediate species or the hydrolysis of dissolved $CuCl_2^-$ (King and Kolar 2000; King et al. 1995a,b, 2001, 2002b). The former process typically is responsible for the formation of the first monolayer or two of Cu_2O, but is unlikely to be responsible for the majority of the relatively thick Cu_2O layer observed experimentally (King et al. 2001, 2002b). Therefore, the most likely reaction for the precipitation of Cu_2O is

$$2CuCl_2^- + H_2O = Cu_2O + 4Cl^- + 2H^+ \qquad (17)$$

Given that water is generally present in excess in the system, the rate of Cu_2O precipitation is taken to be first order with respect to the concentration of $CuCl_2^-$ and is given by

$$-\frac{d[CuCl_2^-]}{dt} = k_2 \max\left[0, ([CuCl_2^-] - [CuCl_2^-]_{sat})\right] \qquad (18)$$

where $[CuCl_2^-]_{sat}$ is the concentration of a saturated solution in equilibrium with Cu_2O and k_2 is the first-order rate constant for the precipitation reaction. The $\max[0, ([CuCl_2^-] - [CuCl_2^-]_{sat})]$ term in Equation (18) prevents Cu_2O from precipitating from an undersaturated solution in the model.

King and Légère (unpublished work) studied the dissolution of Cu_2O powder as a function of pH and Cl^- concentration. The rate was found to be independent of $[Cl^-]$, but to be a function of pH. The rate expression for the dissolution of Cu_2O derived from this work and used in the CCM-UC is

$$-\frac{d[Cu_2O]}{dt} = k_{-2}[Cu_2O] \qquad (19)$$

where $[Cu_2O]$ is the concentration of Cu_2O in units of moles per unit volume of buffer, backfill or host rock, and k_{-2} is the corresponding first-order dissolution rate constant.

Precipitation of $CuCl_2 \cdot 3Cu(OH)_2$ occurs from a supersaturated solution of dissolved Cu(II) (King et al. 2001, 2002b). Dissolution of $CuCl_2 \cdot 3Cu(OH)_2$ is most likely to occur chemically, rather than via a reductive dissolution mechanism, because the high electrical resistivity of geological specimens of atacamite suggests that the surface would not mediate electron-transfer reactions (King and Standlund, unpublished work). Thus, the precipitation and dissolution of $CuCl_2 \cdot 3Cu(OH)_2$ can be described by the reversible reaction

$$4Cu^{2+} + 6OH^- + 2Cl^- = CuCl_2 \cdot 3Cu(OH)_2 \quad (20)$$

The rate of precipitation is given by

$$-\frac{d[Cu^{2+}]}{dt} = k_3 \max\left[0, [Cu^{2+}] - [Cu^{2+}]_{sat}\right] \quad (21)$$

where $[Cu^{2+}]_{sat}$ is the concentration of Cu^{2+} in a saturated solution in equilibrium with $CuCl_2 \cdot 3Cu(OH)_2$ and k_3 is the first-order rate constant for the precipitation reaction. The rate of dissolution of $CuCl_2 \cdot 3Cu(OH)_2$ is given by

$$-\frac{d[CuCl_2 \cdot 3Cu(OH)_2]}{dt} = k_{-3}[CuCl_2 \cdot 3(Cu(OH)_2] \quad (22)$$

where $[CuCl_2 \cdot 3Cu(OH)_2]$ is the concentration of $CuCl_2 \cdot 3Cu(OH)_2$ in units of moles per unit volume of buffer, backfill or host rock and k_{-3} is the corresponding first-order rate constant.

The precipitation of Fe(II) is also included in the model as an unidentified Fe(II) secondary phase ($Fe(II)_{ppt}$). If the rate of dissolution of Fe(II) from ferrous mineral phases in the repository exceeds the rate at which the Fe(II) is subsequently oxidized by reaction with O_2 or Cu^{2+}, the secondary Fe(II) phase will precipitate if the dissolved ferrous ion concentration exceeds the solubility of the secondary phase, as given by

$$Fe(II)_{aq} = Fe(II)_{ppt} \quad (23)$$

The kinetic expressions for the rates of precipitation and dissolution are given by

$$-\frac{d[Fe(II)_{aq}]}{dt} = k_7 \max\left[0, ([Fe(II)_{aq}] - [Fe(II)_{aq}]_{sat}\right] \quad (24)$$

and

$$-\frac{d[Fe(II)_{ppt}]}{dt} = k_{-7}[Fe(II)_{ppt}] \quad (25)$$

where $[Fe(II)_{aq}]_{sat}$ is the concentration of $Fe(II)_{aq}$ in a saturated solution in equilibrium with the $Fe(II)_{ppt}$ phase and k_7 and k_{-7} are the respective first-order rate constants.

2.1.4 Sorption and Desorption

Dissolved Cu(II) adsorbs strongly on sodium bentonite (Ryan and King 1994) and could adsorb on other mineral surfaces within the repository and geosphere. On the other hand, cuprous species in the form of anionic $CuCl_2^-$ species do not adsorb (King et al. 1992, 2001, 2002b).

It is common to model the adsorption of radionuclides on clay using equilibrium linear isotherms (Cook 1988), since the concentration of species is small compared with the cation-exchange

capacity of the clay and sorption and desorption are assumed to be fast relative to the rate of diffusion. In the case of the corrosion of copper in buffer material, however, experimental studies have shown that the total concentration of copper in the buffer close to the corroding surface equals or exceeds the cation-exchange capacity of Na-bentonite (King et al. 1992, Litke et al. 1992). Consequently, it is unlikely that the adsorption behaviour is linear (i.e., the ratio of dissolved to adsorbed concentrations of Cu^{2+} is constant) over the entire concentration range of interest. Equilibrium adsorption studies on loose and compacted Na-bentonite suggest that a Langmuir-type isotherm is more appropriate (Ryan and King 1994). In addition, the rate of desorption of Cu^{2+} from Na-bentonite is much slower than its rate of adsorption. Modelling studies suggest that the adsorption/desorption of diffusing Cu^{2+} on compacted Na-bentonite is not at equilibrium (King et al. 1996).

The adsorption and desorption of Cu^{2+} on bentonite, and other mineral surfaces can be described by

$$Cu^{2+} + 2Y^{-} = CuY_2 \tag{26}$$

where Y^{-} represents a singly charged adsorption site and CuY_2 an adsorbed species. Mathematically, this process is modelled using a kinetic Langmuir expression, with the rate of adsorption given by

$$-\frac{d[Cu^{2+}]}{dt} = k_4[Cu^{2+}]([CuY_2]_{max} - [CuY_2]) \tag{27}$$

where, for the Langmuir expression, the rate of adsorption is proportional to both the concentration of dissolved Cu^{2+} and the concentration of vacant surface sites ($[CuY_2]_{max}$ - $[CuY_2]$), where $[CuY_2]_{max}$ is the maximum surface coverage of adsorbed copper, and k_4 is the second-order adsorption rate constant. The rate of desorption is proportional to the concentration of adsorbed Cu(II)

$$\frac{d[Cu^{2+}]}{dt} = k_{-4}[CuY_2] \tag{28}$$

where k_{-4} is the desorption rate constant.

2.1.5 Microbial Effects

There is now a growing body of evidence that indicates that microbial activity does not occur or will be severely limited in highly compacted bentonite (Masurat et al. 2007; Pedersen 2000; Stroes-Gascoyne et al. 2006, 2007). Although the physiological reason for this lack of activity is uncertain, it is believed to result either from the low water activity (a_W) in both unsaturated and saturated bentonite or from the physical effects of the swelling pressure developed in saturated bentonite. Of particular importance for a DGR in sedimentary rock is the fact that microbial activity can be suppressed in compacted bentonite by saline pore fluids, even at bentonite dry densities as low as about 0.8 $Mg \cdot m^{-3}$ (i.e., an effective montmorillonite dry density (EMDD) of about 0.7 $Mg \cdot m^{-3}$, Stroes-Gascoyne et al. 2006). Together, this evidence indicates that microbial activity close to the UFC will not occur at any stage during the evolution of the repository environment. Therefore, biofilm formation on the container surface will not occur.

Although the possibility of microbial activity close to the container can be excluded, it is possible that microbial activity might occur elsewhere in the repository. For example, in the absence of saline pore fluids, microbial activity is possible in saturated bentonite-based sealing materials with an EMDD of <1.4 $Mg \cdot m^{-3}$ (Stroes-Gascoyne et al. 2006). Under these circumstances, MIC is possible if aggressive metabolic by-products produced remotely diffuse to the UFC surface (King et al. 2002a, 2004).

Remote microbial activity may have a number of effects on the corrosion of copper UFC. The extent of corrosion and SCC due to the diffusion of aggressive metabolic by-products, such as HS^-, NO_2^-, acetate, and ammonia, has been shown to be minimal (King and Kolar 2005, 2006b; King et al. 2003, 2004). However, aerobic bacteria may be responsible for the consumption of a significant fraction of the initially trapped O_2 in the repository (King and Kolar 2006b), especially in light backfill material which has a low EMDD and contains a large fraction of the O_2 inventory because of the low compaction moisture content.

A simple treatment is used in the CCM-UC to simulate the consumption of O_2 by aerobic bacteria, compared with the more-complex treatment used in the CCM-MIC model (King et al. 2002a). In the CCM-UC.1.1, the effect of microbial consumption of O_2 is simulated using the following simplified reaction

$$O_2 \xrightarrow{\text{aerobes}} 2H_2O \tag{29}$$

for which the rate of O_2 consumption is assumed to follow a simple first-order rate expression, given by

$$-\frac{dc_0}{dt} = k_9 c_0 \theta(S - S_{MIC}) \tag{30}$$

where k_9 is the corresponding first-order rate constant, S_{MIC} is the minimum degree of saturation for microbial activity, and $\theta(x)$ is a step function equal to 1 for $x > 0$, and to 0 for $x \leq 0$. The value of S_{MIC} corresponds to a value of a_W of 0.96, a value shown to correspond to the that below which the vast majority of bacteria are inactive (Brown 1990) and below which there is no microbial activity in compacted bentonite (Stroes-Gascoyne et al. 2006, 2007).

2.1.6 Mass Transport of Dissolved and Gaseous Species

Because of the low hydraulic conductivity of the host sedimentary rock and of the clay-based sealing materials within the repository, mass transport of O_2 to, and of Cu^{2+} and $CuCl_2^-$ away from, the UFC surface will occur by diffusion only. Advection will not occur at such low hydraulic conductivities ($<10^{-12}$ to 10^{-13} $m \cdot s^{-1}$). Furthermore, since uniform corrosion does not involve the spatial separation of anodic and cathodic sites, electrochemical potential gradients parallel and perpendicular to the UFC will be minimal and, hence, migration of ions will also not occur.

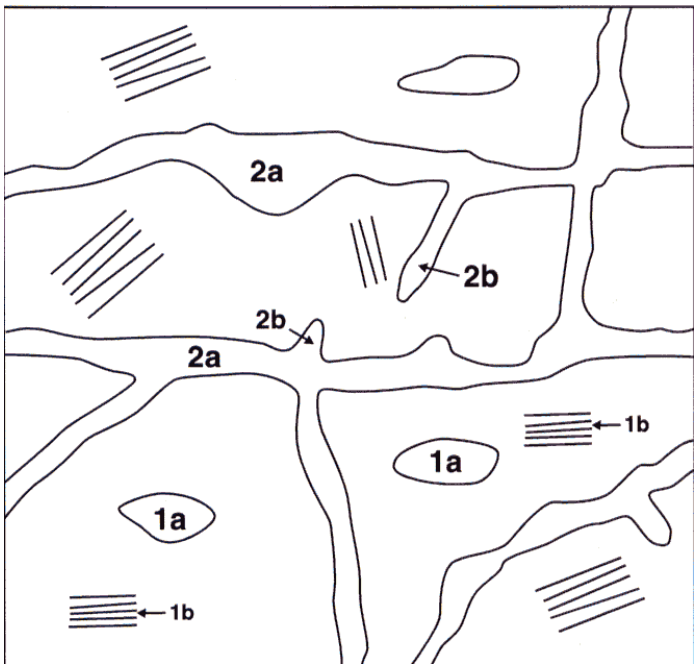

Figure 1: Schematic Representation of the Distribution of Pore Space for the Equivalent Porous Media in the Copper Corrosion Model. The inaccessible porosity is represented by isolated pores (1a) and inter-lamellar regions (1b). The accessible porosity is divided between through (2a) and dead-end (2b) pores.

For mass-transport purposes, the buffer, backfill, and host rock are treated as equivalent porous media. Each different material is described by a total porosity (ε) and a tortuosity factor τ_f. In turn, the total porosity is divided between an accessible porosity (ε_a) and the non-accessible porosity (ε_{na}), the latter representing isolated pores and the inter-lamellar spaces between clay particles too small for the diffusing species to access (Figure 1, King et al. 1996). The accessible porosity is divided between the effective (or through-) porosity for mass transport (ε_e) and the storage porosity (ε_s).

In saturated systems, the effective diffusion coefficient (D_e) is given by (Cook 1988, King et al. 1996)

$$D_e = \tau_f \varepsilon_e D \qquad (31)$$

where D is the diffusion coefficient in bulk solution.

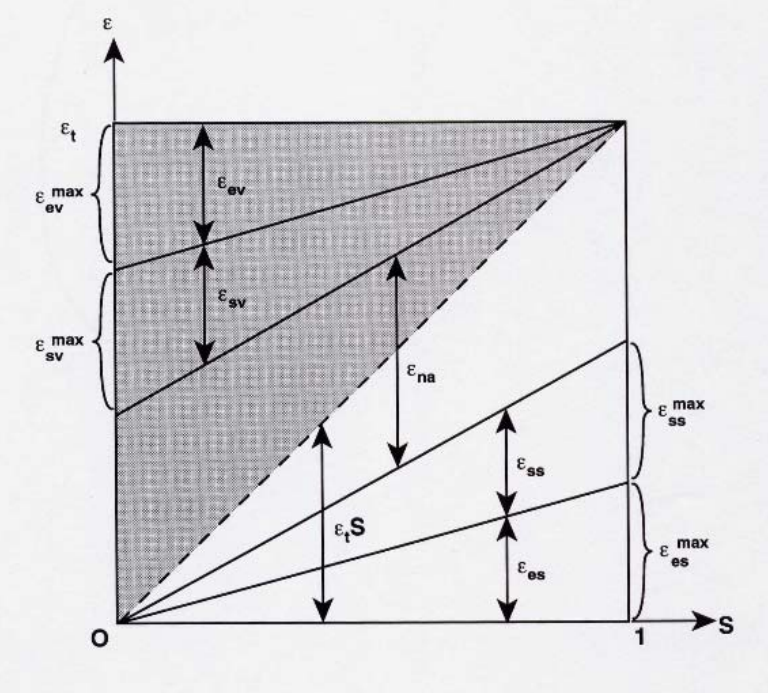

Figure 2: Variation of the Effective and Storage Porosity in the Vapour and Solution Phases in Unsaturated Equivalent Porous Media (King et al. 1996).

In unsaturated systems, diffusion of solutes that can partition into the vapour phase may occur through both solution-filled and vapour-filled pores. Of the species considered in the model, only oxygen will have any significant vapour-phase mass transport component in unsaturated media. Conversely, species that do not significantly partition into the vapour phase will diffuse only through the solution-filled pores.

Figure 2 shows the dependence of the effective, storage, and non-accessible porosities for both the vapour-filled (subscript v) and solution-filled (subscript s) pores. For an equivalent porous medium, the mean solution-filled porosity is proportional to the degree of saturation (S) and the mean vapour-filled porosity is proportional to (1-S). However, the vapour-filled porosity is not continuous, i.e., regions of vapour-filled pores will be separated by regions of solution-filled pores. Consequently, the diffusion coefficient of gaseous O_2 in unsaturated soils is found not to be proportional to (1-S) but to $(1-S)^3$ (Collin and Rasmuson 1988). The effective diffusion coefficients of dissolved and gaseous species in unsaturated equivalent porous media are given, therefore, by

$$D_{es} = \tau_f \varepsilon_e S D \qquad (32a)$$

and

$$D_{ev} = \tau_f \varepsilon_e (1-S)^3 D_a \qquad (32b)$$

respectively, where D_a is the diffusion coefficient of the gaseous species (specifically O_2) in air and it is implicitly assumed that the tortuosity factors for vapour-filled and solution-filled pores are equal.

2.2 EFFECT OF ENVIRONMENTAL PARAMETERS

2.2.1 Salinity

Based on the limited amount of information available to date, deep groundwaters in Ordovician sedimentary deposits tend to be more saline than those at an equivalent depth in the crystalline rock of the Canadian Shield (McMurray 2004, King 2005a). For example, at 500-1000 m, sedimentary deposits have a range of salinities of 200,000-300,000 mg/L total dissolved solids, compared with 2,000-30,000 mg/L for Canadian Shield groundwaters (Figure 3, McMurray 2004). Both sets of groundwaters are predominantly Ca/Na-based chloride solutions, with Cl^- ion concentrations in sedimentary deposits in the range 50,000-150,000 mg/L (1.5-4.4 mol·dm^{-3}).

The high groundwater and pore-water Cl^- concentration will have a number of effects on the corrosion behaviour of copper UFC, including:

1. the speciation of dissolved copper and the solubility of corrosion products,
2. the potential for microbial activity, and
3. the overall likelihood of various forms of corrosion

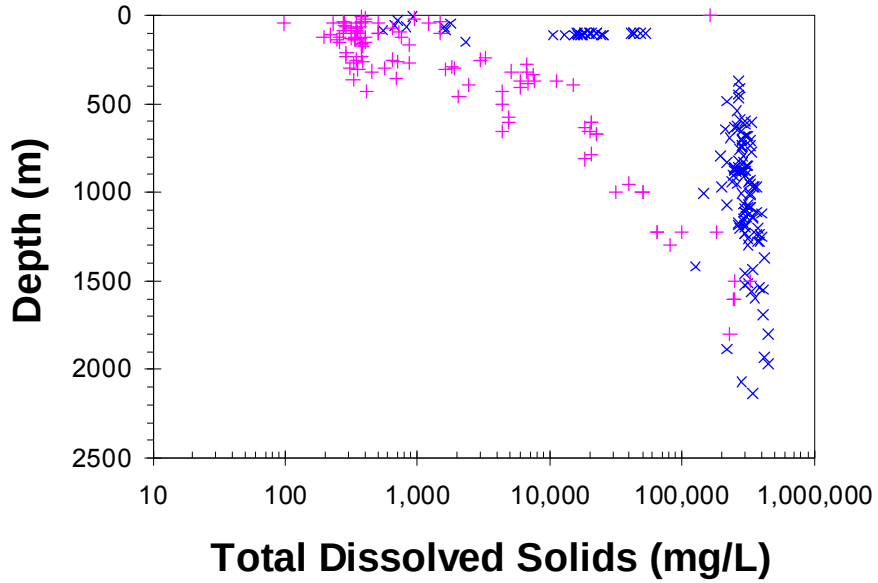

Figure 3: Comparison of the Variation of the Total Dissolved Solids Content with Depth for Michigan Basin and Canadian Shield Groundwaters (after McMurray 2004). + Canadian Shield, X Ordovician Sedimentary.

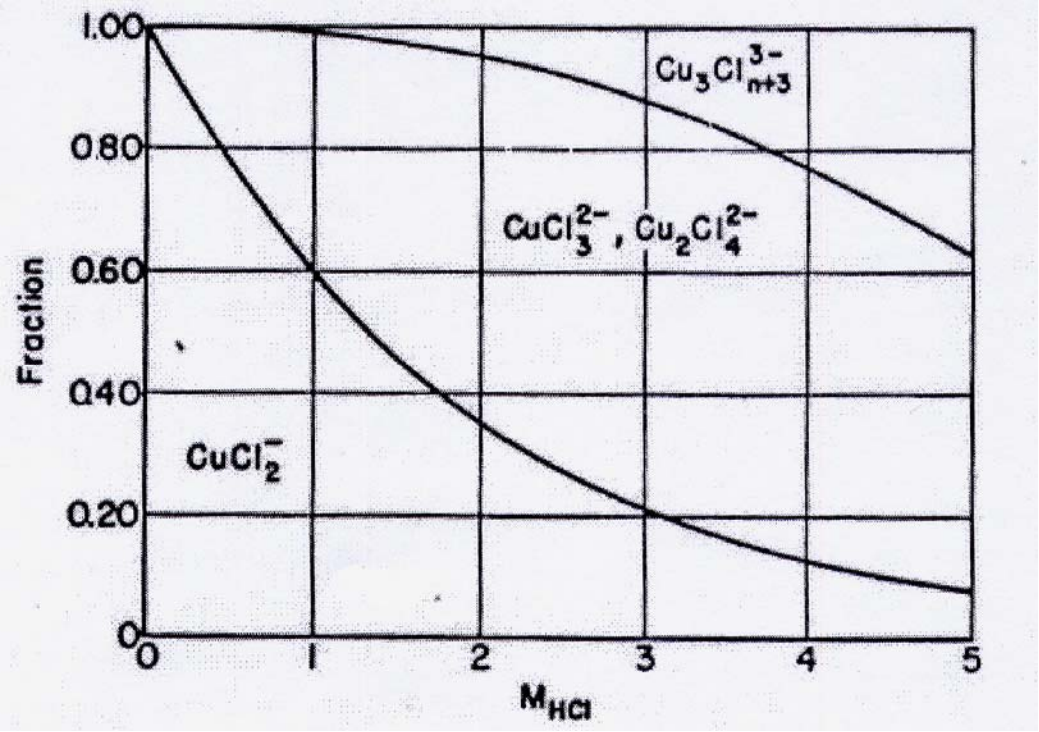

Figure 4: Relative Distribution of Cuprous-Chloro Complexes as a Function of Chloride Concentration in Hydrochloric Acid Solution (Fritz 1980).

Chloride ions stabilize cuprous species in the form of $Cu_xCl_y^{(x-y)}$ complex ions (Fritz 1980, 1981, 1982; Sharma and Millero 1990). With increasing Cl^- concentration successively higher complexes become increasingly more stable. For example, based on the data in Figure 4, $CuCl_2^-$ species predominate for Cl^- concentrations up to ~1.5 mol·dm^{-3}, with a mixture of $CuCl_3^{2-}$ and $Cu_2Cl_4^{2-}$ predominating at higher Cl^- concentrations. Thus, although $CuCl_2^-$ species would be expected to predominate in Canadian Shield groundwaters, the higher complexes would be expected in sedimentary groundwaters.

The overall stability of cuprous species will also be affected by the chloride concentration. The rate constant for the oxidation of Cu(I) by dissolved O_2 decreases with increasing Cl^- concentration (Sharma and Millero 1988). Thus, the more-saline Ordovician sedimentary groundwaters will tend to stabilize Cu(I) to a greater extent than Canadian Shield groundwaters. In turn, the stabilization of Cu(I)-Cl^- complexes will increase the solubility of Cu_2O, resulting in less precipitation.

Microbial activity in compacted bentonite is also affected by the pore-water salinity (Stroes-Gascoyne et al. 2006, 2007). By comparing the number of culturable microbes after exposure to bentonite compacted with saline pore water to that in the as-received material, Stroes-Gascoyne et al. (2006, 2007) were able to show that a pore-water salinity of ≥100 g/L was sufficient to suppress microbial activity in compacted bentonite with dry densities >0.8 Mg·m^{-3}. The threshold salinity for the suppression of microbial activity decreased with

increasing bentonite density. This effect is clearly related to the decrease in water activity with increasing salinity. This effect cannot be explained by an effect of buffer swelling pressure on microbial activity, since the swelling pressure decreases with increasing salinity. Quite clearly, therefore, microbial activity is suppressed due to an increase in the osmotic potential at high pore-water salinity.

The overall effect of high salinity on the corrosion of copper UFC is to induce general corrosion and to suppress localized corrosion and SCC. Therefore, the container would be expected to corrode more uniformly in a repository in sedimentary deposits than under similar conditions in the Canadian Shield. The threat from SCC will also be diminished because of the apparent inhibitive effect of Cl^- on the SCC of copper (Ikeda and Litke 2000; King 1996; King et al. 2001, 2002b).

2.2.2 Degree of Saturation

In addition to potentially higher salinity, another difference between the Ordovician sedimentary deposits and the crystalline host rock of the Canadian Shield is the significantly lower hydraulic conductivity of the shale and limestone deposits (Golder 2003, King 2005a, Mazurek 2004). Hydraulic conductivities of these formations are expected to be of the order of 10^{-12} m·s^{-1}. As a consequence, DGR saturation times could be of the order of tens of thousands of years, resulting in a significant period of unsaturated conditions.

King (2006) reviewed the effect of unsaturated conditions on the corrosion of copper UFC. The degree of saturation of the repository will affect the corrosion behaviour of the UFC in a number of ways, including:

1. a period of dry conditions on the container surface, followed by the deliquescence of surface salts and impurities,
2. rapid supply of O_2 to the container surface through unsaturated sealing materials and the slow transport of corrosion products and other species away from the UFC, and
3. the location and duration of microbial activity in the repository.

Aqueous electrochemical reactions, such as those described in Section 2.1.1, require the presence of liquid water to enable ionic conduction. The thickness of adsorbed water layers increases with increasing relative humidity (RH), reaching a thickness of a few nm at 100% RH, equivalent to a few hundred water layers (Lee and Staehle 1997, Nagano et al. 1998). However, water films as thin as 1-10 water layers are sufficient to support electrochemical reactions and, hence, corrosion (Leygraf and Graedel 2000). Typically, measurable corrosion is observed above a critical RH value of 60-70% (Shreir 1976), which can be related to a threshold degree of saturation of the buffer and backfill materials (King 2006). When wetting of the surface does occur it does so through a process known as deliquescence, in which salts absorb moisture from the vapour phase at a critical RH for a given temperature (King 2006).

In the absence of an aqueous electrolyte, the UFC may be subject to dry-air oxidation (King 2006). However, for the range of expected temperatures, the rate of oxidation is small, with the maximum depth of penetration calculated to be <0.1 μm (King 2006).

Desiccation of the buffer and backfill materials will also affect the rate of mass transport of species to and from the container surface. As described in Section 2.1.6, species that can partition into the gas phase (specifically O_2) will diffuse rapidly through the vapour-filled pores

under unsaturated conditions. Conversely, dissolved species will diffuse more slowly as the interconnectedness of solution-filled pores will be diminished.

Finally, as described in Section 2.1.5, microbial activity will only occur if there is sufficient water available to support metabolic processes. Typically, most bacteria are inactive below a water activity of 0.96 (Brown 1990; Stroes-Gascoyne et al. 2006, 2007), which can be related to a critical degree of saturation of the buffer or backfill material.

2.2.3 Temperature

The temperature within the repository will increase following closure due to the radiogenic heating from the waste inside the containers. The maximum container surface temperature will depend on a number of factors, including the spacing of the containers, the physical arrangement and properties of the buffer and backfill, and the burn-up and age of the fuel. Typically, however, the repository is designed such that the maximum temperature will not exceed a value of ~120°C, above which alteration of the smectite clay minerals can occur (Nagra 2002).

Based on the constraint imposed by the need to avoid thermal alteration of the bentonite, a maximum container surface temperature of 100°C has been specified (Maak 2006). Figure 5 shows an assumed time dependence for the container surface temperature and at a hypothetical fracture location in the far field used by King and Kolar (2006a) in an analysis of the evolution of the corrosion behaviour of a copper UFC in a typical design for a DGR in crystalline rock. The temperatures profiles for UFC in a sedimentary repository are likely to be similar.

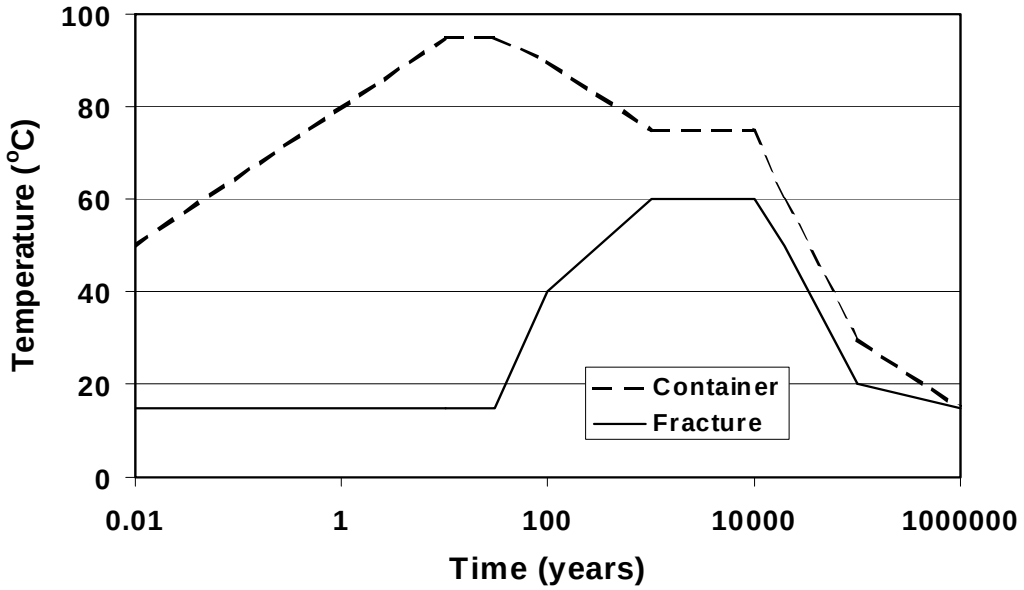

Figure 5: Assumed Time Dependence of the Temperature at the Container Surface and at a Fracture in the Far Field (King and Kolar 2006a).

Most physical, chemical, electrochemical, and mass-transport processes occurring in the repository are temperature dependent. Typically, the rates of processes increase with increasing temperature, although the temperature sensitivity varies. The mathematical treatment of the dependence on temperature of the different processes in the model are described in more detail in Section 4.1.6.

2.2.4 Redox Conditions

Redox conditions within the repository will evolve over time. Initially, air trapped in the voids of the buffer and backfill sealing materials will create relatively oxidizing conditions, but as the O_2 is consumed by corrosion, by aerobic microbial activity, and by reaction with ferrous and other oxidisable materials in the repository, the conditions will become more reducing. Once all of the O_2, and the Cu(II) species produced by oxidation of Cu(I) by O_2, have been consumed corrosion of the copper UFC will cease.

2.2.5 Radiation

Radiolysis of pore water in the bentonite buffer surrounding the container could potentially generate oxidising and reducing radiolysis products. However, since the outer copper shell would require the use of a thick C-steel inner vessel for structural support, the external radiation field will be below that found to have an effect on the corrosion of copper (Shoesmith and King 1999). Therefore, radiation effects are not considered further.

2.3 REACTION SCHEME ADOPTED FOR CCM-UC.1.1

Figure 6 shows the reaction scheme used in the CCM-UC.1.1. This reaction scheme incorporates all of the important electrochemical, redox, precipitation/dissolution, sorption/ desorption, and mass-transport processes for the uniform corrosion of copper in compacted buffer material. Each of the rate constants (denoted by k in Figure 6) have been defined in Section 2.1. The mass-transport processes are denoted by the “J” terms in the figure.

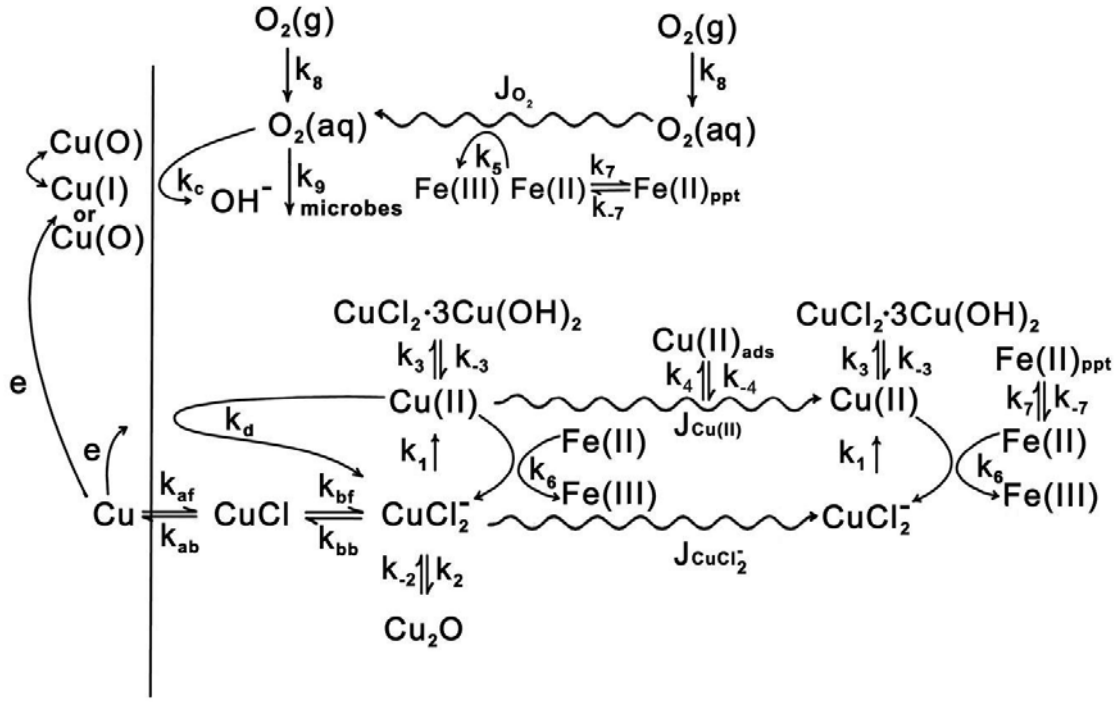

Figure 6: Reaction Scheme for the Copper Corrosion Model for Uniform Corrosion CCM-UC.1.1.

3. UNDERLYING ASSUMPTIONS IN THE MODEL

There are a number of assumptions implicitly and explicitly included in the CCM-UC.1.1. Table 1 lists each assumption and the expected significance of the assumption on the prediction of the long-term uniform corrosion behaviour of copper UFC.

As noted in the table and elsewhere in the text, each of these assumptions is considered to be reasonable and is based on either a theoretical analysis or experimental observation. None of these assumptions results in a non-conservative prediction of container lifetimes.

Table 1: Assumptions Included in the CCM-UC.1.1.

Assumption	Basis
The reaction scheme in Figure 6 is an adequate representation of the mechanism of the uniform corrosion of copper used fuel containers.	This reaction scheme is based on an extensive experimental program and has been partially validated by comparison of predictions with the results of experimental studies (King et al. 1995c, King and Kolar 2006a).
The predominant dissolved cuprous species is $CuCl_2^-$.	This species will predominate during much of the initial period of corrosion, until such time that the pore-water $[Cl^-]$ exceeds ~1.5 mol·dm^{-3}. Although higher Cu(I)-Cl^- complexes will predominate at high $[Cl^-]$, corrosion is expected to be minimal at this time.
The tortuosity factor of the vapour-filled and solution–filled pores is the same.	Both gaseous and dissolved species will diffuse through the same porous network. During the unsaturated phase, water will preferentially occupy the smaller-diameter pores. Any effect on the effective diffusion coefficient of dissolved or gaseous species is expected to be minimal.
The buffer and backfill sealing materials and the host sedimentary rock can be treated using an equivalent porous medium model.	This assumption is considered realistic given the pore structure of these materials. Discrete fractures are not expected to be present.
Microbial activity ceases below a water activity of 0.96.	Although some species of microbe are known to survive at lower water activities, there is extensive experimental evidence to support this threshold value (Stroes-Gascoyne et al. 2006, 2007).
Sulphide is not produced in significant quantities in the repository and, hence, copper is thermodynamically stable in the absence of O_2 and Cu(II).	In the presence of HS^-, copper is thermodynamically unstable in H_2O. Calculations using the CCM-MIC code show that minimal amounts of HS^- are expected to be formed in the repository, with virtually none reaching the container surface (King and Kolar 2006b).
Precipitated corrosion products do not protect or passivate the surface.	Corrosion products are assumed to act only as a sink for dissolved Cu(I) and Cu(II) and not to protect the surface from dissolution. Some protection of the surface is to be expected. Corrosion rates predicted by the model will be conservative.

continued ….

Table 1: Assumptions Included in the CCM-UC.1.1 (concluded).

Assumption	Basis
The corrosion potential is determined only by the rates of the uniform dissolution of copper and of the cathodic reduction of O_2 or Cu(II).	Localized separation of anodic and cathodic reactions could result in more-positive values of E_{CORR}. However, there is no experimental evidence to suggest that anodic and cathodic sites are permanently separated (King and Kolar 2000).
Cupric species are reduced on the copper surface.	In many natural, aerated systems, Cu(II) rather than O_2 is the primary oxidant (King et al. 2001, 2002b). Since the rate of oxidation of Cu(I) to Cu(II) by O_2 is rapid, Cu(II) is predicted to be the primary oxidant for copper UFC. Excluding Cu(II) reduction would be non-conservative.

4. MATHEMATICAL ASPECTS

4.1 MATHEMATICAL CONSTRUCTION OF MODEL

4.1.1 Reaction-Diffusion Equations

The CCM-UC.1.1 model is based on a series of ten one-dimensional reaction-diffusion equations, one for each of the species considered in the reaction mechanism illustrated in Figure 6, namely: gaseous and dissolved O_2 (concentrations c_A and c_0, respectively), dissolved $CuCl_2^-$ (c_1), precipitated Cu_2O (c_2), dissolved Cu(II) (c_3), precipitated $CuCl_2{\cdot}3Cu(OH)_2$ (c_4), adsorbed Cu(II) (c_5), Cl^- ions (c_6), and dissolved and precipitated Fe(II) (c_7 and c_8, respectively). The notation used for the concentration of each of these species is summarized in Table 2. The ten equations are:

$$\frac{\partial\left[(1-S)\varepsilon_a c_A\right]}{\partial t} = \frac{\partial}{\partial x}\left(\tau_f (1-S)^3 \varepsilon_e D_A \frac{\partial c_A}{\partial x}\right) - \varepsilon_a S k_8 (c_0^{sat} - c_0)(1-S)c_A \tag{33a}$$

$$\varepsilon_a \frac{\partial(S c_0)}{\partial t} = \frac{\partial}{\partial x}\left(\tau_f \varepsilon_e S D_0 \frac{\partial c_0}{\partial x}\right) - \varepsilon_a S\left[\frac{k_1}{4} c_0 c_1 + k_5 c_0 c_7 + k_9 c_0 \theta(S - S_{MIC})\right] + \varepsilon_a S k_8 (c_0^{sat} - c_0)(1-S)c_A \tag{33b}$$

$$\varepsilon_a \frac{\partial(S c_1)}{\partial t} = \frac{\partial}{\partial x}\left(\tau_f \varepsilon_e S D_1 \frac{\partial c_1}{\partial x}\right) + \varepsilon_a S\left[-k_1 c_0 c_1 + k_6 c_3 c_7 - k_2 \max(0, c_1 - c_1^{sat})\right] + 2k_{-2} c_2 \tag{33c}$$

$$\frac{\partial c_2}{\partial t} = \varepsilon_a S \frac{k_2}{2} \max(0, c_1 - c_1^{sat}) - k_{-2} c_2 \tag{33d}$$

$$\varepsilon_a \frac{\partial (S c_3)}{\partial t} = \frac{\partial}{\partial x}\left(\tau_f \varepsilon_e S D_3 \frac{\partial c_3}{\partial x} \right) + \varepsilon_a S \left[k_1 c_0 c_1 - k_6 c_3 c_7 - k_3 \max(0, c_3 - c_3^{sat}) - k_4 c_3 (c_5^{max} - c_5) \rho_d \right] + 4 k_{-3} c_4 + k_{-4} c_5 \rho_d \tag{33e}$$

$$\frac{\partial c_4}{\partial t} = \varepsilon_a S \frac{k_3}{4} \max(0, c_3 - c_3^{sat}) - k_{-3} c_4 \tag{33f}$$

$$\rho_d \frac{\partial c_5}{\partial t} = \varepsilon_a S k_4 c_3 (c_5^{max} - c_5) \rho_d - k_{-4} c_5 \rho_d \qquad \text{for } c_5 < c_5^{max} \tag{33g}$$

$$\varepsilon_a \frac{\partial (S c_6)}{\partial t} = \frac{\partial}{\partial x}\left(\tau_f \varepsilon_e S f_{D6} D_6 \frac{\partial c_6}{\partial x} \right) + \varepsilon_a S \left[2 k_1 c_0 c_1 - 2 k_6 c_3 c_7 + 2 k_2 \max(0, c_1 - c_1^{sat}) - \frac{k_3}{2} \max(0, c_3 - c_3^{sat}) \right] + 2 k_{-3} c_4 - 4 k_{-2} c_2 \tag{33h}$$

$$\varepsilon_a \frac{\partial (S c_7)}{\partial t} = \frac{\partial}{\partial x}\left(\tau_f \varepsilon_e S D_7 \frac{\partial c_7}{\partial x} \right) + \varepsilon_a S A_F [R_0 e^{-\alpha_F t} + R_1] - \varepsilon_a S [4 k_5 c_0 c_7 + k_6 c_3 c_7 + k_7 \max(0, c_7 - c_7^{sat})] + k_{-7} c_8 \tag{33i}$$

$$\frac{\partial c_8}{\partial t} = \varepsilon_a S k_7 \max(0, c_7 - c_7^{sat}) - k_{-7} c_8 \tag{33j}$$

where ρ_d is the dry density of the porous medium given by $\rho_d = (1-\varepsilon_a)\rho_p$, where ρ_p is the particle density of the solid skeleton, and all of the other symbols are defined in Section 2.1 or Figure 6.

In addition to the mass-balance equations for the chemical species, a heat-conduction equation is included in the model, given by

$$\rho C \frac{\partial T}{\partial t} = \frac{\partial}{\partial x}\left(K \frac{\partial T}{\partial x} \right) \tag{34}$$

where ρ is the wet bulk density, T is the temperature, and C and K are the bulk specific heat and the bulk thermal conductivity, respectively.

Table 2: Notation for the Concentration of Each of the Chemical Species and Temperature Used in the Copper Corrosion Model for Uniform Corrosion (CCM-UC.1.1).

Species	Notation
Gaseous O_2	c_A
Dissolved O_2	c_0
Dissolved $CuCl_2^-$	c_1
Precipitated Cu_2O	c_2
Dissolved Cu^{2+}	c_3
Precipitated $CuCl_2 \cdot 3Cu(OH)_2$	c_4
Adsorbed Cu(II)	c_5
Dissolved Cl^-	c_6
Dissolved Fe(II)	c_7
Precipitated Fe(II)	c_8
Temperature	T

4.1.2 Model Geometry

The physical system being simulated is defined by the corrosion model geometry. A series of layers is used to represent the various buffer and backfill sealing materials, the excavation-disturbed zone(s) (EDZ) surrounding the rooms and tunnels, and the host geological media. An arbitrary number of layers can be defined. For example, more than one layer can be defined for a given material to simulate spatially dependent saturation behaviour (King and Kolar 2006a). Alternatively, the EDZ or host geological media can be represented by more than one layer if available information suggests that the properties are distinct.

The layers that are generally considered in the corrosion model are (King and Kolar 2006a):

1. inner buffer material (compacted 100% bentonite)
2. outer buffer (50:50 bentonite:sand)
3. dense backfill (5:25:70 bentonite:lake clay:aggregate)
4. light backfill (50:50 bentonite:sand)
5. EDZ (shale or limestone)
6. host geological media (shale or limestone)

Table 3 defines the layer-dependent properties in the model. Not all layers will be applicable to all DGR designs. Also not all parameters will be important for all layers. For example, some of the materials will have minimal Fe(II) mineral content, so that the parameters $c_7(x,0)$ and A_F are not defined.

Table 3: Media-dependent Parameters in the CCM-UC.1.1.

Symbol	Definition
L	Layer thickness
ε_a	Accessible porosity, $\varepsilon_a = \varepsilon_e + \varepsilon_s$
ε_e	Effective porosity for mass transport
ε_s	Storage porosity. Equivalent to that part of the connected porosity that does not participate directly in diffusion, e.g., the dead-end pores, but is still accessible to the dissolved species.
τ_f	Tortuosity factor
$\rho(S)$	Bulk density
$c_A(x,0)$	Initial concentration of gaseous O_2
$c_0(x,0)$	Initial concentration of dissolved O_2
$c_6(x,0)$	Initial concentration of Cl^- ions
$c_7(x,0)$	Initial concentration of dissolved Fe(II)
c_5^{max}	Maximum concentration of adsorbed Cu^{2+}
k_9	First-order rate constant for the consumption of O_2 by aerobic microbes
A_F	Surface area of exposed Fe(II) mineral phase
C(S)	Bulk specific heat
K(S)	Bulk thermal conductivity
S(t)	Time-dependent degree of saturation
S_{MIC}	Minimum degree of saturation at which microbial activity can occur

The layers that define the model geometry are bounded on both sides. The left-hand boundary is the container surface. The right hand boundary is a location within the host geological media at which chemical and thermal conditions are constant.

4.1.3 Boundary Conditions

Each of the mass-balance equations (for diffusing species only) and the heat conduction equation are solved subject to mathematical boundary conditions for the left- and right-hand boundaries. Electrochemical expressions are used for the left-hand boundary conditions for those species reacting on, or being produced at, the container surface (i.e., dissolved O_2, $CuCl_2^-$, Cu^{2+}, and Cl^-). Gaseous O_2 and Fe(II) do not react on the container surface and are, hence, assigned zero-flux left-hand boundary conditions. A zero-concentration or constant-concentration is assumed at the right-hand boundary for all species, depending upon the composition of the groundwater. Time-dependent, externally defined temperatures are used for the left- and right-hand boundary conditions for the heat-conduction equation. Table 4 summarizes the nature of the boundary conditions for the different species.

Table 4: Nature of the Boundary Conditions for the Diffusing Species in CCM-UC.1.1. *

Species	Left-hand Boundary Condition	Right-hand Boundary Condition
O_2(g)	Zero flux	Zero flux
O_2(aq)	Electrochemical	Constant concentration
$CuCl_2^-$	Electrochemical	Zero concentration
Cu^{2+}	Electrochemical	Zero concentration
Cl^-	Electrochemical	Constant concentration
Fe(II)(aq)	Zero flux	Constant concentration
T	Time dependent	Time dependent

* Non-diffusing species are Cu_2O(s), $CuCl_2.3Cu(OH)_2$(s), Cu(II)(ads) and Fe(II)(s).

Electrochemical expressions are used as the left-hand boundary condition for those species that react on the container surface, namely; O_2(aq), $CuCl_2^-$, Cu^{2+}, and Cl^-. The respective electrochemical reactions are:

$$Cu + Cl^- \underset{k_{ab}}{\overset{k_{af}}{\rightleftharpoons}} CuCl_{ads} + e^- \qquad (35a)$$

$$CuCl_{ads} + Cl^- \underset{k_{bb}}{\overset{k_{bf}}{\rightleftharpoons}} CuCl_2^- \qquad (35b)$$

$$O_2 + 2H_2O + 4e^- \xrightarrow{k_c} 4OH^- \qquad (35c)$$

$$Cu^{2+} + 2Cl^- + e^- \xrightarrow{k_d} CuCl_2^- \qquad (35d)$$

The rate of the anodic dissolution of Cu as $CuCl_2^-$ (Reactions (35a) and (35b)) is given by

$$i_a = n_a F\left(k_a [Cl^-]^2 \exp\left(\frac{F}{RT}(E - E_a^0) \right) - k_{bb}[CuCl_2^-] \right) \qquad (36)$$

where the various symbols have been defined previously in Section 2.1.

The equivalent expressions for the reduction of O_2 (Reaction (35c)) and of Cu^{2+} (Reaction (35d)) are

$$i_c = -n_c F k_c [O_2] \exp\left(-\frac{\alpha_c F}{RT}(E - E_c^0) \right) \qquad (37)$$

and

$$i_d = -n_d F k_d [Cu^{2+}] \exp\left(-\frac{\alpha_d F}{RT}(E - E_d^0)\right) \tag{38}$$

where again the various symbols have been defined previously in Section 2.1.

The rate of the anodic reaction must equal the sum of the rates of the two cathodic reactions

$$i_a(t) + i_c(t) + i_d(t) = 0 \tag{39}$$

These currents are also related to the diffusive fluxes at $x = 0_+$ of the dissolved species participating in the interfacial reactions. Thus,

$$i_a(t) = -n_a F \tau_f \varepsilon_e D_1 \frac{\partial c_1(0,t)}{\partial x} \tag{40}$$

$$i_a(t) = 2n_a F \tau_f \varepsilon_e D_6 \frac{\partial c_6(0,t)}{\partial x} \tag{41}$$

$$i_c(t) = -n_c F \tau_f \varepsilon_e D_0 \frac{\partial c_0(0,t)}{\partial x} \tag{42}$$

$$i_d(t) = -n_d F \tau_f \varepsilon_e D_3 \frac{\partial c_3(0,t)}{\partial x} \tag{43}$$

Combining Equations (40) and (41) gives one more boundary condition

$$D_1 \frac{\partial c_1(0,t)}{\partial x} + 2D_6 \frac{\partial c_6(0,t)}{\partial x} = 0 \tag{44}$$

Under freely corroding conditions, E(t) corresponds to the corrosion potential (E_{CORR}), which can be determined by rearranging Equation (36)

$$E_{CORR} \equiv E(t) = E_a^0 + \frac{RT}{F} \ln\left[\frac{i_a(t) + n_a F k_{bb} c_1(0,t)}{n_a F k_a [c_6(0,t)]^2}\right] \tag{45}$$

Substituting Equation (45) into Equations (37) and (38) gives two further boundary conditions

$$\frac{-i_c(t)}{F} = n_c k_c c_0(0,t) \left[\frac{n_a k_a [c_6(0,t)]^2}{\frac{i_a(t)}{F} + n_a k_{bb} c_1(0,t)}\right]^{\alpha_c} \exp\left[\frac{\alpha_c F}{RT}(E_c^0 - E_a^0)\right] \tag{46}$$

and

$$\frac{-i_d(t)}{F} = n_d k_d c_3(0,t)\left[\frac{n_a k_a [c_6(0,t)]^2}{\frac{i_a(t)}{F} + n_a k_{bb} c_1(0,t)}\right]^{\alpha_d} \exp\left[\frac{\alpha_d F}{RT}(E_d^0 - E_a^0)\right] \quad (47)$$

4.1.4 Initial Conditions

Initial conditions are required for all of the species in the model for each of the mass-transport layers. The initial conditions are summarized in Table 5. For those species that are initially present in the repository or host rock, such as $O_2(g)$, $O_2(aq)$, Cl^-, and Fe(II),

$$c_i(x,0) = c_{iL} \quad (48)$$

where c_i is c_A, c_0, c_6, and c_7 and L = 1, …..n represents the n mass-transport layers.

For those species not initially present, such as all of the copper species and secondary-phase precipitated Fe(II),

$$c_i(x,0) = 0 \quad (49)$$

where i = 1, 2, 3, 4, 5, and 8.

The initial temperature in the repository is assumed to be equal to that of the host rock

$$T(x,0) = T_{rock} \quad (50)$$

Table 5: Initial Conditions for Each of the Species Included in the CCM-UC.1.1.

Notation	Species	Initial Condition
c_A	$O_2(g)$	$c_A(x,0) = c_{AL}$
c_0	$O_2(aq)$	$c_0(x,0) = c_{0L}$
c_1	$CuCl_2^-$	$c_1(x,0) = 0$
c_2	Cu_2O	$c_2(x,0) = 0$
c_3	Cu^{2+}	$c_3(x,0) = 0$
c_4	$CuCl_2 \cdot 3Cu(OH)_2$	$c_4(x,0) = 0$
c_5	Cu(II)(ads)	$c_5(x,0) = 0$
c_6	Cl^-	$c_6(x,0) = c_{6L}$
c_7	Fe(II)(aq)	$c_7(x,0) = c_{7L}$
c_8	Fe(II)(ppt)	$c_8(x,0) = 0$
T	-	$T(x,0) = T_{rock}$

4.1.5 Degree of Saturation

The degree of saturation S of the various layers in the model will change with time as a consequence of the changing thermal profile in the repository and the ingress of groundwater from the host rock. The time-dependent saturation behaviour of the repository is a complex phenomenon involving coupled thermal-hydraulic-mechanical (THM) processes, and is not explicitly modelled in the CCM-UC.1.1. However, the following effects of the time-dependent saturation process are taken into account in the model:

1. the effect of S(x,t) on the diffusion coefficient of dissolved species (Equation (32a)),
2. the effect of S(x,t) on the diffusion coefficient of gaseous O_2 (Equation (32b)),
3. the variation in the specific heat and thermal conductivity on S(x,t) and, hence, the effect on the spatial- and temporal-dependent temperature within the repository,
4. the change in the concentration of dissolved and gaseous species as a consequence of the changing volume of the pore solution,
5. the effect of moisture content on the rate of the microbial consumption of O_2, and
6. the effect of the interfacial moisture content on the rate of electrochemical surface reactions.

Furthermore, although S is assumed to be spatially uniform within a given model layer, variations in the degree of saturation within a given material can be simulated by assigning more than one layer in the model to a given material.

Since water is not one of the species included in the model, the degree of saturation cannot be explicitly predicted by the current version of the CCM. Instead, the time dependence of S for each layer is inputted as an external parameter. Values for S can be derived from the results of large-scale heated experiments or from detailed THM models. For example, Figure 7 shows the time-dependent saturation used for the inner and outer buffer layers by King and Kolar (2006a). In these simulations, the degree of saturation was specified for three layers of inner buffer and two layers of outer buffer material.

The effect of S on the microbial consumption of O_2 and on the diffusion coefficients of gaseous and dissolved species have been discussed in Sections 2.1.5 and 2.1.6, respectively.

Because electrochemical corrosion reactions require the presence of an aqueous phase or, as a minimum, a thin surface liquid film, corrosion may not be possible in compacted media at low degrees of saturation. To account for this phenomenon, the interfacial rate constants for the various electrochemical reactions considered in the model are dependent on the surface moisture content h_k as follows:

$$
\begin{aligned}
&k_i = 0 \qquad \text{for} \qquad h_k \le h_{k,min} \\
&k_i = \frac{h_k - h_{k,min}}{h_{k,max} - h_{k,min}} k_{i,max} \qquad \text{for} \qquad h_{k,min} < h_k < h_{k,max} \; ; \quad i = a, bb, c, d \\
&k_i = k_{i,max} \qquad \text{for} \qquad h_k \ge h_{k,max}
\end{aligned}
\tag{51}
$$

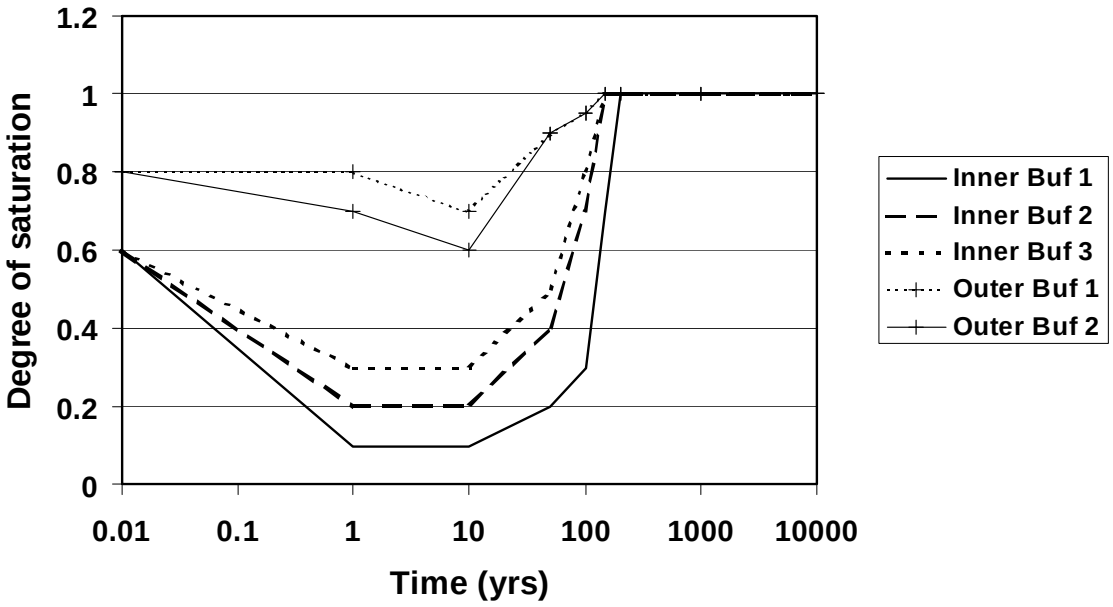

Figure 7: Time Dependence of the Degree of Saturation for the Inner and Outer Buffer Layers (King and Kolar 2006a). The initial degree of saturation is shown at a time of 0.01 years.

where $k_{i,max}$ is the maximum value of the respective rate constant corresponding to fully saturated conditions, and $h_{k,min}$ and $h_{k,max}$ are the values of h_k between which k_i is assumed to grow linearly from 0 to its maximum value. The values of $h_{k,min}$ and $h_{k,max}$ are defined by the threshold relative humidity for atmospheric corrosion (60-70% RH, Shreir 1976).

4.1.6 Temperature

Unlike the degree of saturation, the spatial and temporal dependence of the temperature is calculated in the code. The heat-conduction equation (Equation (34)) is solved subject to time-dependent temperature boundary conditions for any arbitrary initial temperature profile. The time dependence of the left-hand and right-hand boundary temperatures are inputted as a separate file (e.g., Figure 5).

In the solution of the heat-conduction equation, the dependence of the bulk density (ρ), the heat capacity of the composite medium (C), and the thermal conductivity (K) on the degree of saturation is explicitly taken into account. The bulk density is related to the density of water (ρ_w) and of the solid skeleton (particle density ρ_p) by

$$\rho = \varepsilon_a S \rho_w + (1 - \varepsilon_a)\rho_p \qquad (52)$$

The bulk heat capacity is related to the heat capacity of the solid matrix (C_p) and of water (C_w) by

$$C = \frac{C_w \varepsilon_a S \rho_w + C_p (1-\varepsilon_a)\rho_p}{\varepsilon_a S \rho_w + (1-\varepsilon_a)\rho_p} \tag{53}$$

The temperature dependence of C_w and ρ_w are calculated in the code, and C_p and ρ_p are assumed to be independent of temperature within the temperature range of interest (10-100°C). Finally, the dependence of K on S is read into the model as an input file.

Temperature-dependent expressions are used for all of the diffusion coefficients, rate constants, saturated concentrations, and standard potentials in the model. Arrhenius-type expressions are used for the diffusion coefficients, rate constants, and saturated concentrations, of the form

$$D_i = D_{iR} \exp\left[\frac{\Delta H_{D_i}}{R}\left(\frac{1}{T_R} - \frac{1}{T}\right)\right] \qquad \text{for i = A, 0, 1, 3, 6, 7} \tag{54}$$

$$k_i = k_{iR} \exp\left[\frac{\Delta H_{k_i}}{R}\left(\frac{1}{T_R} - \frac{1}{T}\right)\right] \qquad \text{for i = } \pm 2, \pm 3, \pm 4, 5, 6, \pm 7, 8, 9, a, bb, c, d \tag{55a}$$

$$\log k_1 = 11.38 - \frac{2064}{T} - 3.69\left(\frac{c_6}{1 - 0.1103 c_6}\right)^{1/2} + 0.73\left(\frac{c_6}{1 - 0.1103 c_6}\right) \tag{55b}$$

$$R_i = R_{iR} \exp\left[\frac{\Delta H_{R_i}}{R}\left(\frac{1}{T_R} - \frac{1}{T}\right)\right] \qquad \text{for i = 0, 1} \tag{56}$$

$$\alpha_F = \alpha_{FR} \exp\left[\frac{\Delta H_{\alpha_F}}{R}\left(\frac{1}{T_R} - \frac{1}{T}\right)\right] \tag{57}$$

$$c_i^{sat} = c_{iR}^{sat} \exp\left[\frac{\Delta H_i^{sat}}{R}\left(\frac{1}{T_R} - \frac{1}{T}\right)\right] \qquad \text{for i = 3, 7} \tag{58}$$

$$c_0^{sat} = 0.02046 - 1.702 \times 10^{-4} T + 4.764 \times 10^{-7} T^2 - 4.451 \times 10^{-3} T^3 \tag{59}$$

$$c_1^{sat} = c_{1R}^{sat}\left(\frac{c_6}{1 \text{mol} \cdot \text{dm}^{-3}}\right)^2 \exp\left[\frac{\Delta H_1^{sat}}{R}\left(\frac{1}{T_R} - \frac{1}{T}\right)\right] \tag{60}$$

where ΔH are the activation energies for the various diffusion coefficients, rate constants, and solubilities, the subscript R refers to room temperature (25°C), and all other parameters have been previously defined.

The standard potentials are linearly related to temperature according to

$$E_i^0 = E_{iR}^0 + \Delta E_i^0 (T - T_R) \qquad \text{for i = a, c, d} \tag{61}$$

4.2 NUMERICAL SOLUTION OF REACTION-DIFFUSION EQUATIONS

The CCM-MIC.0 code is based on the reaction-diffusion equations solver TRANSIENT (Kolar 2006). This section is based to a large extent on the theory part of the manual for the current version TRANSIENT V2.54.

4.2.1 General Statement of the Problem

The set of reaction-diffusion equations defined in Section 4.1.1 (Equations (33a) to (33j) and (34)) constitute a set of eleven coupled partial differential equations of the parabolic type which can be written in the form

$$\varepsilon_k(x)\frac{\partial c_k(x,t)}{\partial t} = \frac{\partial}{\partial x}\left(\alpha_k(x,T(x,t))\frac{\partial c_k(x,t)}{\partial x}\right) + R_k(c_i(x,t),x,t) \qquad (62)$$

where x (position) and t (time) are the independent variables, c_i, i=1,...,11 denotes all the dependent variables (the concentrations of the 10 species and c_{11} being the temperature T), k=1,...,11 represents the equation number, $\varepsilon_k(x)$ is either ε or ρC and is always a piece-wise constant, α_k is the intrinsic diffusivity for the k-th dependent variable, and R_k the reaction terms which are non-linear functions of the concentrations c_i and also of position (via ε, ρ, etc.) and possibly of time). For non-diffusive equations, α_k in Equation (62) is identically equal to zero. For equations with piece-wise constant material characteristics ε and τ_f, α_k is also a piece-wise constant with discontinuities only at the inter-media interfaces. These discontinuities have to be accounted for properly (see Equations (79) to (81) below).

The respective boundary conditions for the diffusive species are of the form

$$\beta_{k,b}\left(\frac{\partial c_i(x_b,t)}{\partial x}, c_i(x_b,t), t\right) = 0 \qquad \text{b = left, right} \qquad (63)$$

Here the explicit time dependence originates from the temperature dependence of the electrochemical rate constants and of the standard potentials. For the non-diffusive species, no special boundary conditions are needed. The “bulk” (homogeneous) non-diffusive equations can be used without any change as the formal boundary conditions for $x = x_{left}$, x_{right} because in the non-diffusive equations, x is just a parameter. One has to define “boundary conditions” for all equations, because all have to be treated by the computer code in the same way when solved simultaneously.

4.2.2 Spatial Grid

The spatial grid for the CCM-UC.1.1 has an increasing grid spacing from the left-hand boundary (x = 0) to the right-hand boundary. The grid is finest at the container surface, where the interfacial electrochemical reactions occur and where the concentration gradients are generally the steepest. Inside each medium, the grid spacing increases from left to right according to a geometrical progression. The quotient of this progression is different in each layer.

To build the grid, the grid spacings Δx_λ at the layer interfaces are specified such that $\Delta x_\lambda < \Delta x_{\lambda+1}$. The quotient for the λ-th layer of thickness L_λ is calculated as follows:

$$q_l = \frac{L_l - 2\Delta x_{l-1}}{L_l - 2\Delta x_l} > 1 \tag{64}$$

Then Δx_λ are adjusted slightly (from left to right) so that there are an exact number of grid intervals, n_λ, within the λ-th layer using the above quotient for the ratio of any two adjacent grid intervals. Using these slightly adjusted values of Δx_λ, the grid points in the λ-th layer are:

$$x_{left,l} + \Delta x_l \frac{q_l^i - 1}{q_l - 1}; \quad i = 0,1,\ldots,n_l \tag{65}$$

where $x_{left,\lambda}$ is the position of the beginning of the λ-th layer.

4.2.3 Discretization

Both x and t have to be discretized. There are $N = n_1+n_2+\ldots+n_\lambda+1$ grid points x_j given by Equation (65), and an *a priori* unspecified number of time instants t_ℓ (ℓ = 0, 1, ...). Values of $c_k(x,t)$ are calculated only at these discrete values of x and t. The concentration and temperature values at these discrete points and times will be referred to as both $c_k(j, \ell)$ and $c_k(x_j,t_\ell)$.

All of the derivatives in Equations (62) and (63) are replaced by suitable difference formulae. For the time derivative at the j-th grid point, we use the following replacement

$$\frac{\partial c_k(x,t)}{\partial t} \rightarrow \frac{c_k(j,\ell+1)-c_k(j,\ell)}{t_{\ell+1}-t_\ell} \tag{66}$$

Here we assume that the solution is already known at t_ℓ and we want to advance it to the next time instant, $t_{\ell+1}$. On the right-hand side (RHS) of Equation (62), we can use the usual 3-point central difference formulae for the given type of grid in a differencing scheme of general implicitness (1 - τ), where $0 \le \tau \le 1$; mixing together τ parts of the "old" solution at t_ℓ with (1 - τ) parts of the “new” (to be computed) solution at $t_{\ell+1}$. Let us introduce

$$\bar{c}_i(j) = \tau c_i(j,\ell)+(1-\tau)c_i(j,\ell+1), \tag{67}$$

and substitute this expression for all $c_i(x,t)$ on the RHS of Equation (62), and discretize it using suitable difference formulae for the derivatives. Note that $\bar{c}_k(j)$ as defined in Equation (67) corresponds to $c_k(x_j,t_\tau)$ at time $t_\tau = t_\ell + \tau(t_{\ell+1} - t_\ell) = \tau t_{\ell+1} + (1 - \tau)t_\ell$, as calculated by linear interpolation between $c_k(j,\ell)$ and $c_k(j,\ell + 1)$. Correspondingly, the last term in Equation (62) is replaced by $R_k(\bar{c}_i(j), x_j, t_\tau)$ in this differencing scheme.

Usually, the best choice for τ should be $\tau = 0.5$, corresponding to $t_\tau = (t_\ell + t_{\ell+1})/2$. Note that, in this case only, the error of the difference formula in Equation (66) is second order with respect to the time step; otherwise, it is first order. A τ value of 0.5 gives the Crank-Nicholson scheme which, for equidistant grids, is of the second order both in space and time, and for pure diffusion is stable for arbitrary time-step size. It is also stable for large time steps for many types of the reaction term $R_k(c_i(x,t),x,t)$. A τ value of 1 gives the fully explicit scheme, which is stable only for very small time steps, and $\tau = 0$ gives a fully implicit scheme, stable for arbitrary time steps. Thus, $\tau = 0.5$ should give the smallest error due to discretization. However, if there are any problems with convergence, a value of $\tau < 0.5$ should be used.

As α_k = constant in Equation (62) in the interior of each medium, we can use the following 3-point central difference formulae at the j-th grid point:

$$\frac{\partial^2 c_i(x,t)}{\partial x^2} \to \frac{2}{\Delta_- + \Delta_+}\left\{\frac{\bar{c}_i(j+1) - \bar{c}_i(j)}{\Delta_+} + \frac{\bar{c}_i(j-1) - \bar{c}_i(j)}{\Delta_-}\right\}, \tag{68}$$

$$\frac{\partial c_i(x,t)}{\partial x} \to \frac{1}{\Delta_- + \Delta_+}\left\{[\bar{c}_i(j+1) - \bar{c}_i(j)]\frac{\Delta_-}{\Delta_+} - [\bar{c}_i(j-1) - \bar{c}_i(j)]\frac{\Delta_+}{\Delta_-}\right\}. \tag{69}$$

where $\Delta_- = x_j - x_{j-1}$ and $\Delta_+ = x_{j+1} - x_j$. These formulae were obtained by requiring that the first three terms of the Taylor series at x_j of the RHS of Equations (68) and (69) are correct (i.e., equal to the respective LHS). The lowest-order error term of the difference formulae (68) and (69) are $\frac{1}{3}(\Delta_+ - \Delta_-)\bar{c}_i'''$ and $\frac{1}{6}\Delta_+\Delta_-\bar{c}_i'''$, respectively. Here $\bar{c}_i''' = \frac{\partial^3 c_i}{\partial x^3}(x_\tau, t_\tau)$. If $\Delta_- = \Delta_+ = h$, Equations (68) and (69) would be equivalent to the standard equidistant formulae with the error term $O(h^2)$.

Similarly, for j = 0 the following 3-point forward difference formula can be used with Equations (39) to (43)

$$\frac{\partial c_k(x,t)}{\partial x} \to \frac{1}{\Delta_1}\left[-\frac{q+2}{q+1}c_k(0,l+1) + \frac{1+q}{q}c_k(1,l+1) - \frac{1}{q(q+1)}c_k(2,l+1)\right] \tag{70}$$

where $\Delta_1 = x_1 - x_0$, $\Delta_2 = x_2 - x_1 = q_1\Delta_1$, and the lowest-order error term is $\frac{1}{6}\Delta_1(\Delta_1 + \Delta_2)c_k'''$. An analogous formula holds for j = N-1, involving q_N and $c_k(j,\ell+1)$ at j = N-3,N-2,N-1.

For interfaces between two media, i.e., if x_j is a grid point at the interface between two media, we have to satisfy the continuity of the diffusive fluxes:

$$\tau_{f-}\varepsilon_- \frac{\partial c_k}{\partial x}(x_{j-}, t) = \tau_{f+}\varepsilon_+ \frac{\partial c_k}{\partial x}(x_{j+}, t), \tag{71}$$

Here τ_{f-} and ε_{-} are the values of τ_f and ε to the left of the interface at x_j, and τ_{f+} and ε_{+} those to the right. The usual way of discretizing Equation (71) is to replace the one-sided derivatives in the above equations by the following *asymmetric* difference formulae

$$\frac{\partial c}{\partial x}(x_{j^-}, t) \rightarrow \frac{c(j, \ell+1) - c(j-1, \ell+1)}{\Delta_-} \tag{72}$$

and

$$\frac{\partial c}{\partial x}(x_{j^+}, t) \rightarrow \frac{c(j+1, \ell+1) - c(j, \ell+1)}{\Delta_+} \tag{73}$$

where c stands for c_k.

However, we prefer to use an alternative (integrational, or mass-balance) approach that proved to give higher precision in cases when a comparison with an analytical solution was possible (Kolar 2006). As explained below, this approach treats all the nodes in the same way, and thus results in discretization that is consistent throughout the whole model. Note that Equation (68) can also be obtained by integrating $\frac{\partial^2 c}{\partial x^2}$ from $x_j - \frac{\Delta_-}{2}$ to $x_j + \frac{\Delta_+}{2}$, dividing the result by the length of the integration interval, and then applying the following *symmetric* difference formulae

$$\frac{\partial c_k}{\partial x}\left(x_j - \frac{\Delta_-}{2}, t\right) \rightarrow \frac{\overline{c}_k(j) - \overline{c}_j(j-1)}{\Delta_-} \tag{74}$$

and

$$\frac{\partial c_k}{\partial x}\left(x_j + \frac{\Delta_+}{2}, t\right) \rightarrow \frac{\overline{c}_k(j+1) - \overline{c}_j(j)}{\Delta_+} \tag{75}$$

Let us assume that $c(j, \ell)$ is approximately constant in the vicinity of each grid point, i.e.,

$$\frac{2}{\Delta_+ + \Delta_-} \int_{x_j - \Delta_-/2}^{x_j + \Delta_+/2} c_k(x, t_\ell)\, dx \rightarrow c_k(j, \ell) \tag{76}$$

and

$$\frac{2}{\Delta_+ + \Delta_-} \int_{x_j - \Delta_-/2}^{x_j + \Delta_+/2} P(c_i(x, t_\ell), x, t_\ell)\, dx \rightarrow P(c_i(j, \ell), x, t_\ell). \tag{77}$$

Then the discretization of Equation (62), as described above for the interior grid points in each medium, is equivalent to the following procedure: integrate Equation (62) from $x_j - \frac{\Delta_-}{2}$ to $x_j + \frac{\Delta_+}{2}$, divide the result by $(\Delta_+ + \Delta_-)/2$ and perform the replacements of Equations (66) and (74) - (77). This amounts to discretizing the integral form of the mass-balance Equation (62).

In order to get consistent discretization throughout the whole sample, let us now apply this procedure at all the grid points, including the inter-media boundaries, and also at the outer boundaries 0 and x_{right}. The only modification for the end points results from the fact that the

integration is one-sided, i.e., from 0 to $\frac{\Delta_+}{2}$ for the left outer boundary, and from $x_{right} - \frac{\Delta_-}{2}$ to x_{right} for the right outer boundary.

Let us now perform this integration (or mass-balance) approach to discretization for the grid nodes on an inter-media boundary x_j. Note that for all equations, the reaction terms can be written in the form

$$R_k = \phi_k + \varepsilon_a \psi_k \tag{78}$$

where ϕ_k and ψ_k are not explicitly dependent on x. We again assume that $c_k(x,t)$ and $R_D(x,t)$ (and thus also ϕ_k and ψ_k) are constant in the small interval (x_j -Δ_-/2, x_j + Δ_+/2) and equal to their values at x_j, $c_k(x,t) = c_k(x_j,t)$. Integrating the diffusive Equations (33) or (34) from x_j - Δ_-/2 to x_j + Δ_+/2 gives

$$\left(\varepsilon_{a-}\frac{\Delta_-}{2}+\varepsilon_{a+}\frac{\Delta_+}{2}\right)\frac{\partial c_k(x_j,t)}{\partial t} = D_k\tau_{f+}\varepsilon_{a+}\frac{\partial c_k}{\partial x}\left(x_j+\frac{\Delta_+}{2},t\right)-D_k\tau_{f-}\varepsilon_{e-}\frac{\partial c_k}{\partial x}\left(x_j-\frac{\Delta_-}{2},t\right)$$

$$+\phi_k\frac{\Delta_-+\Delta_+}{2}+\psi_k\left(\varepsilon_{a-}\frac{\Delta_-}{2}+\varepsilon_{a+}\frac{\Delta_+}{2}\right). \tag{79}$$

Here, we have used the condition of diffusion flux continuity at the interface (Equation (71)). Now dividing both sides of Equation (79) by $\frac{1}{2}(\varepsilon_-\Delta_- + \varepsilon_+\Delta_+)$ and using difference formulae Equation (66), (74) and (75) gives

$$\frac{2D_k}{\Delta_-^2(1+q)\varepsilon_{Interface}}\left\{\frac{\tau_{f+}\varepsilon_{e+}}{q}\left[\bar{c}_k(j+1)-\bar{c}_k(j)\right]-\tau_{f-}\varepsilon_{e-}\left[\bar{c}_k(j)-\bar{c}_k(j-1)\right]\right\}$$

$$+\frac{\varphi_k+\varepsilon_{Interface}\psi_k}{\varepsilon_{Interface}}-\frac{c_k(j,\ell+1)-c_k(j,\ell)}{t_{\ell+1}-t_\ell}=0, \tag{80}$$

where $\varepsilon_{Interface} = \frac{\varepsilon_{a-}+q\varepsilon_{a+}}{1+q}$ and $q = \frac{\Delta_+}{\Delta_-}$.

Note that the reaction term in Equation (80) has exactly the same form as at the interior nodes (Equation (78)) except that ε is replaced by $\varepsilon_{Interface}$. The same result is obtained for those of Equations (33) that are non-diffusing (with the diffusion term absent, or D=0). Discretizing these equations in the same way as the other four above, we get

$$\varphi_k+\varepsilon_{Interface}\psi_k-\frac{c_k(j,\ell+1)-c_k(j,\ell)}{t_{\ell+1}-t_\ell}=0. \tag{81}$$

Unlike the case of inter-media boundaries, at the outer boundaries the integration approach to discretization does not change the form of the discretized boundary conditions for the non-diffusive equations.

4.2.4 Solution of the Resultant Algebraic Equations

Upon performing discretization as indicated above, we get a system of n x N equations of the form

$$F_k^{(j)}(c_i(m,\ell+1),c_i(m,\ell)) \equiv 0, \tag{82a}$$

in n x N unknowns $c_i(m,\ell + 1)$, involving the "old" concentrations, $c_i(m,\ell)$, as known parameters. Here, n=11; k=1,...,n; j = 0,1,..., N - 1; m = 0, 1, 2 for j = 0; m = j - 1, j, j + 1 for $1 \le j \le N - 2$; and m = N - 3, N - 2, N - 1 for j = N -1. For the internal nodes in each medium, the form of $F_k^{(j)}$ is

$$F_k^{(j)} = \sum_{i=0}^{n-1} \mathrm{LIN}(\bar{c}_i(j-1),\bar{c}_i(j),\bar{c}(j+1)) + \frac{P_k(\bar{c}_i(j),x_j,t_\tau)}{\varepsilon_k(x_j)} - \frac{c_k(j,\ell+1)-c_k(j,\ell)}{t_{\ell+1}-t_\ell}, \tag{82b}$$

where LIN( ) represents a linear combination of its arguments. At the inter-media boundaries, $F_k^{(j)}$ is equal to the LHS of Equation (80) or (81).

This set of non-linear algebraic equations can be solved using Spotnitz's (1994) Newton-Raphson (NR) approach, based on Newman's method (Matlosz and Newman 1987, Newman 1973, Nguyen and White 1987, White 1978) as implemented in the TRANSIENT package (Kolar 2006). In this approach, $F_k^{(j)}$ are expanded about a trial point, indicated by $|_0$, using a Taylor series expansion, i.e.,

$$F_k^{(j)} = F_k^{(j)}\big|_0 + \sum_{i=0}^{n-1} \Big\{ A_{k,i}^{(j)} \left[c_i(j-1,\ell+1) - c_i(j-1,\ell+1)\big|_0 \right]$$

$$+ B_{k,i}^{(j)} \left[c_i(j,\ell+1) - c_i(j,\ell+1)\big|_0 \right] + D_{k,i}^{(j)} \left[c_i(j+1,\ell+1) - c_i(j+1,\ell+1)\big|_0 \right] \Big\}, \tag{83}$$

where

$$A_{k,i}^{(j)} = \frac{\partial F_k^{(j)}}{\partial c_i(j-1,\ell+1)}\Big|_0, \tag{84}$$

$$B_{k,i}^{(j)} = \frac{\partial F_k^{(j)}}{\partial c_i(j,\ell+1)}\Big|_0, \tag{85}$$

$$D_{k,i}^{(j)} = \frac{\partial F_k^{(j)}}{\partial c_i(j+1,\ell+1)}\Big|_0. \tag{86}$$

Note that $A_{k,i}^{(j)}$ represents an n x n matrix defined for j = 1 to N - 1, $B_{k,i}^{(j)}$ represents an n x n matrix defined for j = 0 to N - 1, and $D_{k,i}^{(j)}$ represents an n x n matrix defined for j = 0 to N - 2.

Because of the difference formulae used at the boundaries, two more matrices must be defined, as follows:

$$X_{k,i} = \frac{\partial F_k^{(j)}}{\partial c_i(2, \ell+1)}\Big|_0 \qquad \text{for } j=0, \text{and} \tag{87}$$

$$Y_{k,i} = \frac{\partial F_k^{(j)}}{\partial c_i(N-3, \ell+1)}\Big|_0 \qquad \text{for } j=N-1. \tag{88}$$

We can write Equation (83) in matrix form,

$$\mathbf{J}d\mathbf{c} = -\mathbf{F}\Big|_0 \tag{89}$$

where

$$\mathbf{J} = \begin{bmatrix} \mathbf{B}^{(0)} & \mathbf{D}^{(0)} & \mathbf{X} & & \\ \mathbf{A}^{(1)} & \mathbf{B}^{(1)} & \mathbf{D}^{(1)} & & \\ & \cdot & \cdot & \cdot & \\ & \mathbf{A}^{(j)} & \mathbf{B}^{(j)} & \mathbf{D}^{(j)} & \\ & & \cdot & \cdot & \cdot \\ & & \mathbf{Y} & \mathbf{A}^{(N-1)} & \mathbf{B}^{(N-1)} \end{bmatrix}, \quad d\mathbf{c} = \begin{bmatrix} dc^{(0)} \\ dc^{(1)} \\ \cdot \\ dc^{(j)} \\ \cdot \\ dc^{(N-1)} \end{bmatrix}, \quad \mathbf{F}\Big|_0 = \begin{bmatrix} F^{(0)}\Big|_0 \\ F^{(1)}\Big|_0 \\ \cdot \\ F^{(j)}\Big|_0 \\ \cdot \\ F^{(N-1)}\Big|_0 \end{bmatrix},$$

$\mathbf{A}^{(j)}$ is the square matrix with elements $A_{k,i}^{(j)}$; k,i = 0,...,n - 1, etc., d**c** is a column vector with elements $dc_i^{(j)}$ = $c_i(j,\ell + 1) - c_i(j,\ell + 1)|_0$; i = 0,...,N -1 , and $\mathbf{F}^{(j)}|_0$ is a column vector with elements $F_k^{(j)}\Big|_0$; k = 0,...,n - 1.

J and $\mathbf{F}|_0$ are evaluated at some $\mathbf{c}|_0 = \mathbf{c}^{guess}$, and Equation (89) solved for d**c**. If d**c** and $\mathbf{F}|_0$ are less than some specified tolerances, the problem is solved, otherwise $\mathbf{c}^{newguess} = d\mathbf{c} + \mathbf{c}^{oldguess}$ and the process is repeated until convergence is obtained, or signs of divergence or oscillations are detected. In our case, the most suitable initial guess, i.e., the guess for $c_k(j,\ell + 1)$, is obtained by linear extrapolation of $c_k(j,\ell - 1)$ and $c_k(j,\ell)$ to the next time instant $t_{\ell+1}$.

To solve Equation (89) for the unknown $dc_i^{(j)}$, we have modified Spotnitz's (1994) algorithm. First an upper-lower decomposition of **J** is performed to get

$$\mathbf{J}d\mathbf{c} = \mathbf{LU}d\mathbf{c} = -\mathbf{F}|_0 \tag{90}$$

L and **U** can be written as

$$\mathbf{L}=\begin{bmatrix} b^{(0)} & 0 & 0 & & & \\ a^{(1)} & b^{(1)} & 0 & & & \\ & \cdot & \cdot & \cdot & & \\ & & a^{(j)} & b^{(j)} & & \\ & & & \cdot & \cdot & \cdot \\ & & & y & a^{(N-1)} & b^{(N-1)} \end{bmatrix}, \quad \mathbf{U}=\begin{bmatrix} 1 & E^{(0)} & x & & \\ 0 & 1 & E^{(1)} & & \\ & \cdot & \cdot & \cdot & \\ & & 1 & E^{(j)} & \\ & & \cdot & \cdot & \cdot \\ & & & & 1 \end{bmatrix}.$$

Let

$$\mathbf{U}d\mathbf{c} = \xi \tag{91}$$

so that

$$\mathbf{L}\xi = -\mathbf{F}|_0 \tag{92}$$

In the modified algorithm, the Jacobian submatrices (84) through (88), the elements of the **L** and **U** matrices and the components of the ξ vector (using Equation (93)) are calculated simultaneously for each grid node, one grid node at a time, starting from j = 0. For all grid nodes j, the same memory is re-used for the Jacobian submatrices and for $\mathbf{a}^{(j)}$ and $\mathbf{b}^{(j)}$. Similarly, a single n-component vector is used for all $\mathbf{F}^{(j)}|_0$. Only $\mathbf{E}^{(j)}$ and $\xi^{(j)}$ have to be stored for all j. Finally, the back substitution of Equation (91) is done to solve for $d\mathbf{c}^{(j)}$.

4.2.5 Adaptive Time-Stepping Algorithm

An heuristic adaptive time-stepping algorithm (ATSA) is used. This algorithm is used to select the size of the time step $\Delta t_\ell = t_{\ell+1} - t_\ell$. The above described NR algorithm is then used to advance the solution $c_k(j,\ell)$ at t_ℓ to $c_k(j,\ell + 1)$ at $t_{\ell+1}$. The integration has to be started with a small time step to be able to handle the initial rapid variation in various concentrations and any possible initial singularities. As we are interested in the very long-term behaviour, the time step must eventually be increased as much as possible to complete the integration in a reasonable real time. However, a regular increase (e.g., linear or exponential) of the time step is usually not satisfactory because the rate of change of various concentrations changes with time.

The most often-used, and the simplest, adaptive time-stepping algorithm is based on the maximum[1] change in the value of c_k in one time step $\Delta t_\ell = t_{\ell+1} - t_\ell$

$$\Delta c_{max}^{(\ell)} = \max_{j,k}\left(w_k \left| c_k(j,\ell+1) - c_k(j,\ell)\right|\right) \quad . \tag{93}$$

Here w_k are arbitrary weight coefficients that can be introduced for individual species. The algorithm is based on the assumption that $\Delta c_{max}^{(\ell)}$ is roughly proportional to Δt_ℓ. One requires that $\Delta c_{max}^{(\ell)}$ is of the order of a $\Delta c_{max}^{required}$, which is the control quantity of the algorithm and

[1] Alternatively, a suitable average over all grid node j and dependent variables k can be used instead of the maximum in Equation (93). In general, the average is directly proportional to the maximum.

determines the accuracy of the calculation. $\Delta c_{max}^{required}$ is either a constant, a linear or an exponential function of time. If the current value of Δt_ℓ produces $\Delta c_{max}^{(\ell)}$ (as determined by Equation (93)), the new value of the time step (to be used for the next integration step starting at $t = t_{\ell+1}$) is simply[2]

$$\Delta t_{\ell+1} = \Delta t_\ell \cdot \frac{\Delta c_{max}^{required}(t_\ell)}{\Delta c_{max}^{(\ell)}}. \qquad (94)$$

The disadvantage of this simple algorithm is that it always tries to maintain $\Delta c_{max}^{(\ell)}$ close to $\Delta c_{max}^{required}$. This may sometimes lead to a very large number of NR iterations, or even failure of the NR procedure (Equations (89) to (92)) to converge (for some time ranges), because the time step produced by Equation (94) is too large. What is needed is an algorithm that will only ensure that $\Delta c_{max}^{(\ell)}$ does not exceed $\Delta c_{max}^{required}$ (strictly or approximately), but that would allow for $\Delta c_{max}^{(\ell)}$ to be much lower than $\Delta c_{max}^{required}$ whenever convergence problems arise.

The dependence of the number of NR iterations needed to achieve convergence in one integration step, n_{inter}, on the value of Δt_ℓ is usually flat and linear (in terms of the smooth line connecting the centres of consecutive steps of this stepwise dependence) for small values of Δt_ℓ, but then it turns up sharply at a certain value of Δt. Beyond this upturn a small increase in Δt_ℓ may lead to a huge increase in n_{iter} and thus to a prohibitive increase in the CPU time. Ideally, we would want to operate just below this sharp upturn. The problem is that the dependence of n_{iter} on Δt_ℓ is not fixed; it usually varies continually with time as the character of c_k changes.

Thus, our heuristic algorithm is based also on n_{iter}. Actually, the “basic” version of the algorithm (corresponding to strict = -1, where strict is a TRANSIENT input control parameter) is based exclusively on n_{iter}. This basic version uses only one control parameter, N_{iter}, which is the required number of NR iterations in one integration step. The algorithm uses as large a time step as possible such that n_{iter} is, *most of the time*, equal to or less than N_{iter}.

The fastest execution in terms of the CPU time should be achieved with the value of N_{iter} corresponding to the onset of that sharp upturn in the dependence of n_{iter} on Δt_ℓ (averaged over time) discussed above. To see which value of N_{iter} results in the shortest CPU time, different values of N_{iter} should be tried, starting from 2, in otherwise identical runs.

This basic version of our ATSA will thus essentially find the largest $\Delta c_{max}^{(\ell)}$ (as a function of time), compatible with a given value of N_{iter}. Often, this may give sufficient accuracy for smaller values of N_{iter}. To check this, the full version of the algorithm is available (invoked with strict ≥ 0). The full version links $\Delta t_{\ell+1}$ both to N_{iter} and to $\Delta c_{max}^{required}$; $\Delta t_{\ell+1}$ is essentially the smaller of the value given by Equation (94) and the value determined by the basic version of the algorithm as described above. This full version satisfies the requirements for a good ATSA as postulated above; $\Delta c_{max}^{(\ell)}$ never exceeds $\Delta c_{max}^{required}$ (at least not significantly), but it can be arbitrarily small whenever necessary to prevent convergence problems.

[2] If $\Delta c_{max}^{(\ell)}$ exceeds $\Delta c_{max}^{required}$ considerably, one may first want to repeat the current integration step starting at t_ℓ using the reduced time step given by the RHS of Equation (94).

A recommended strategy is to first use the basic version of the algorithm and inspect the resulting $\Delta c_{max}^{(\ell)}$ (shown with monitor = 2 and also always output into the diag file), and then to try the full version with successively smaller $\Delta c_{max}^{required}$ until the results (concentrations as function of time) do not change any more. Of course, using very small values of $\Delta c_{max}^{required}$ can increase the execution time considerably.

The current ATSA is based on the lengths of two previous time steps. From their ratio, and from whether the current number of iterations exceeds N_{iter} or not, the ATSA tries to determine a suitable next time step. This extrapolation is always biased towards larger time steps (it tries to push the step upwards whenever possible). If, for the current time instant, TRANSIENT fails to converge, the time step is reduced, and another attempt at convergence is made. Too many recent failures signify that the time step has been increased too fast. A weighted average of the number of such attempts for all previous time steps is kept in a variable (the weight for the most recent completed time step is ½, for the one before that ¼, and so on - decreased by ½ for each preceding time instant; these weights have nothing to do with the weights of Equation (93)). If everything goes well, the contents of this simple history variable should be one or just slightly above one, most of the time. If the number of failed attempts per time step has grown recently, the value of the history variable stays above 1 for some time. The larger it is, the smaller the upper limit on the maximum allowed time step increase that the algorithm maintains. ATSA usually goes very smoothly, without oscillations in the magnitude of the time step and/or the number of NR iterations, and through any abrupt changes in the evolution of c_k's.

5. SUMMARY

A mechanistically based model has been described for the prediction of the long-term uniform corrosion behaviour of copper used fuel containers in a deep geological repository in sedimentary rock. The reaction scheme used in the model is based on an extensive experimental program with copper materials and includes the following processes: interfacial electrochemical reactions on the container surface, precipitation/dissolution of corrosion products and a secondary ferrous mineral phase, adsorption/desorption of cupric ions on sodium bentonite and other mineral surfaces, redox reactions between O_2 and Cu(I) and Fe(II) species, and the mass transport of reactants to, and of corrosion products away from, the container surface.

Two characteristic features of deep sedimentary host rock are the high groundwater salinity and the low hydraulic conductivity. The high salinity, in particular the high Cl^- concentration, will promote uniform corrosion over localized corrosion or stress corrosion cracking, affect the speciation and solubility of copper corrosion products, and inhibit microbial activity through the decrease in water activity. The low hydraulic conductivity will result in slow saturation of the repository. During the unsaturated period, corrosion may be inhibited by the lack of sufficient water on the container surface. Furthermore, the rates of mass transport of both gaseous and dissolved species will be affected by the unsaturated conditions, as will the extent of microbial activity.

The mathematical basis for the model is a series of eleven reaction-diffusion equations, one for each of the ten chemical species considered and temperature. These equations are solved using finite-difference methods subject to certain initial and boundary conditions. Among the boundary conditions on the container surface are electrochemical expressions that form a mixed-potential model and permit the prediction of the time-dependent corrosion potential and corrosion rate. The model is capable of predicting the time-dependent evolution of environmental conditions within the deep geological repository.

REFERENCES

Bacarella, A.L. and J.C. Griess, Jr. 1973. The anodic dissolution of copper in flowing sodium chloride solutions between 25°C and 175°C. Journal Electrochemical Society 120, 459-465.

Bjorndahl, W.D. and K. Nobe. 1984. Copper corrosion in chloride media. Effect of oxygen. Corrosion 40, 82-87.

Bonfiglio, C.H., H.C. Albaya and O.A. Cobo. 1973. The kinetics of the anodic dissolution of copper in acid chloride solutions. Corrosion Science 13, 717-724.

Braun, M. and K. Nobe. 1979. Electrodissolution kinetics of copper in acidic chloride solutions. Journal Electrochemical Society 126, 1666-1671.

Brown, D.A. 1990. Microbial Water Stress Physiology. John Wiley, Chichester.

Collin, M. and A. Rasmuson. 1988. A comparison of gas diffusivity models for unsaturated porous media. Soil Sci. Soc. Am. J. 52, 1559-1565.

Cook, A.J. 1988. A desk study of surface diffusion and mass transport in clay. British Geological Survey Report, WE/88/34.

Crundwell, F.K. 1992. The anodic dissolution of copper in hydrochloric acid solutions. Electrochimica Acta 37, 2707-2714.

Deslouis, C., B. Tribollet, G. Mengoli and M.M. Musiani. 1988a. Electrochemical behaviour of copper in neutral aerated chloride solution. I. Steady-state investigation. Journal Applied Electrochemistry 18, 374-383.

Deslouis, C., B. Tribollet, G. Mengoli and M.M. Musiani. 1988b. Electrochemical behaviour of copper in neutral aerated chloride solution. II. Impedance investigation. Journal Applied Electrochemistry 18, 384-393.

Dhar, H.P., R.E. White, G. Burnell, L.R. Cornwell, R.B. Griffin and R. Darby. 1985. Corrosion of Cu and Cu-Ni alloys in 0.5M NaCl and in synthetic seawater. Corrosion 41, 317-323.

Faita, G., G. Fiori and D. Salvadore. 1975. Copper behaviour in acid and alkaline brines-I. Kinetics of anodic dissolution in 0.5M NaCl and free-corrosion rates in the presence of oxygen. Corrosion Science 15, 383-392.

Fritz, J.J. 1980. Chloride complexes of CuCl in aqueous solution. Journal Physical Chemistry 84, 2241-2246.

Fritz, J.J. 1981. Representation of the solubility of CuCl in solutions of various aqueous chlorides. J. Phys. Chem. 85, 890-894.

Fritz, J.J. 1982. Solubility of cuprous chloride in various soluble aqueous chlorides. Journal Chemical Engineering Data 27, 188-193.

Gierszewski, P., J. Avis, N. Calder, A. D'Andrea, F. Garisto, C. Kitson, T. Melnyk, K. Wei and L. Wojciechowski. 2004. Third Case Study - Postclosure Safety Assessment. Ontario Power Generation, Nuclear Waste Management Division Report 06819-REP-01200-10109-R00. Toronto, Canada.

Golder. 2003. LLW geotechnical feasibility study Western Waste Management Facility, Bruce Site, Tiverton, Ontario. Golder Associates report to Ontario Power Generation, Report 021-1570.

Hurlen, T. 1961a. Electrochemical behaviour of copper in acid chloride solution. Acta Chemical Scand. 15, 1231-1238.

Hurlen, T. 1961b. Dissolution of copper by oxidation agents in acid chloride solution. Acta Chemical Scand. 15, 1239-1245.

Ikeda, B.M. and C.D. Litke. 2000. The effect of oxidant flux, nitrite concentration and chloride concentration on the stress corrosion cracking behaviour of non-welded and electron-beam welded copper. Ontario Power Generation Nuclear Waste Management Division Report 06819-REP-01200-10049-R00.

Johnson, L.H., D.M. LeNeveu, D.W. Shoesmith, D.W. Oscarson, M.N. Gray, R.J. Lemire and N.C. Garisto. 1994. The disposal of Canada's nuclear fuel waste: the vault model for postclosure assessment. Atomic Energy of Canada Limited Report, AECL-10714, COG-93-4.

Johnson, L.H., D.M. LeNeveu, F. King, D.W. Shoesmith, M. Kolar, D.W. Oscarson, S. Sunder, C. Onofrei and J.L. Crosthwaite. 1996. The disposal of Canada's nuclear fuel waste: a study of postclosure safety of in-room emplacement of used CANDU fuel in copper containers in permeable plutonic rock: volume 2: vault model. Atomic Energy of Canada Limited Report, AECL-11494-2, COG-96-552-2.

Kato, C., B.G. Ateya, J.E. Castle and H.W. Pickering. 1980a. On the mechanism of corrosion of Cu-9.4Ni-1.7Fe alloy in air saturated aqueous NaCl solution. I. Kinetic investigations. Journal Electrochemical Society 127, 1890-1896.

Kato, C., J.E. Castle, B.G. Ateya, and H.W. Pickering. 1980b. On the mechanism of corrosion of Cu-9.4Ni-1.7Fe alloy in air saturated aqueous NaCl solution. II. Composition of the protective surface layer. Journal Electrochemical Society 127, 1897-1903.

Kear, G., B.D. Barker, F.C. Walsh. 2004. Electrochemical corrosion of unalloyed copper in chloride media – a critical review. Corros. Sci. 46, 109-135.

King, F. 1991. Magnetite spherule golf ball. J. Irreproducible Results, 36, 19.

King, F. 1996. The potential for stress corrosion cracking of copper containers in a Canadian nuclear fuel waste disposal vault. Atomic Energy of Canada Limited Report, AECL-11550, COG-96-94.

King, F. 2005a. Evolution of environmental conditions in a deep geological repository in the sedimentary rock of the Michigan Basin, Ontario. Ontario Power Generation Nuclear Waste Management Division Report 06819-REP-01300-10102-R00.

King, F. 2005b. Overview of the corrosion behaviour of copper and steel used-fuel containers in a deep geological repository in the sedimentary rock of the Michigan Basin, Ontario. Ontario Power Generation, Nuclear Waste Management Division Report 06819-REP-01300-10101-R00.

King, F. 2006. Review and gap analysis of the corrosion of copper containers under unsaturated conditions. Ontario Power Generation, Nuclear Waste Management Division Report 06819-REP-01300-10124-R00.

King, F. 2007. Overview of a carbon steel container corrosion model for a deep geological repository in sedimentary rock. Nuclear Waste Management Organization Report No.: NWMO TR-2007-01.

King, F. and M. Kolar. 1995. Prediction of the lifetimes of copper nuclear waste containers under restrictive mass-transport and evolving redox conditions," CORROSION/95, NACE International, Houston, TX, paper #425.

King, F. and M. Kolar. 1996. A numerical model for the corrosion of copper nuclear fuel waste containers," Mats. Res. Soc. Symp. Proc. 412, Materials Research Society, Pittsburgh, PA, 555-562.

King, F and M. Kolar. 1997a. The effect of geosphere conditions on the lifetimes of copper containers. Atomic Energy of Canada Limited Report, AECL-11717, COG-96-565.

King, F. and M. Kolar. 1997b. Corrosion of copper containers prior to saturation of a nuclear fuel waste disposal vault. Atomic Energy of Canada Limited Report, AECL-11718, COG-96-566.

King, F. and M. Kolar. 2000. The copper container corrosion model used in AECL's second case study. Ontario Power Generation, Nuclear Waste Management Division Report 06819-REP-01200-10041-R00.

King, F. and M. Kolar. 2004. Theory manual for the copper corrosion model for stress corrosion cracking of used fuel disposal containers CCM-SCC.0. Ontario Power Generation, Nuclear Waste Management Division Report 06819-REP-01300-10095-R00.

King, F. and M. Kolar. 2005. Preliminary assessment of the stress corrosion cracking of used fuel disposal containers using the CCM-SCC.0 model. Ontario Power Generation, Nuclear Waste Management Division Report 06819-REP-01300-10103-R00.

King, F. and M. Kolar. 2006a. Simulation of the consumption of oxygen in long-term *in situ* experiments and in the third case study repository using the copper corrosion model CCM-UC.1.1. Ontario Power Generation, Nuclear Waste Management Division Report, 06819-REP-01300-10084-R00.

King, F. and M. Kolar. 2006b. Consequences of microbial activity for corrosion of copper used fuel containers – analyses using the CCM-MIC.0.1 code. Ontario Power Generation, Nuclear Waste Management Division Report 06819-REP-01300-00120-R00. Toronto, Ontario.

King, F. and Y. Tang. 1998. The anodic dissolution of copper in chloride-sulphate groundwaters. Ontario Hydro Report No. 06819-REP-01200-0058 R00.

King, F., C.D. Litke and S.R. Ryan. 1992. A mechanistic study of the uniform corrosion of copper in compacted Na-montmorillonite/sand mixtures. Corrosion Science 33, 1979-1995.

King, F., M.J. Quinn and C.D. Litke. 1995a. Oxygen reduction on copper in neutral NaCl solution. J. Electroanal. Chem. 385, 45-55.

King, F., C.D. Litke and Y. Tang. 1995b. Effect of interfacial pH on the reduction of oxygen on copper in neutral $NaClO_4$ solution. J. Electroanal. Chem. 384, 105-113.

King, F., C.D. Litke, M.J. Quinn and D.M. LeNeveu. 1995c. The measurement and prediction of the corrosion potential of copper in chloride solutions as a function of oxygen concentration and mass-transfer coefficient. Corrosion Science 37, 833-851.

King, F., M. Kolár and D.W. Shoesmith. 1996. Modelling the effects of porous and semi-permeable layers on corrosion processes. CORROSION/96, (NACE International, Houston, TX), Paper no. 380.

King, F., S.R. Ryan and C.D. Litke. 1997. The corrosion of copper in compacted clay. Atomic Energy of Canada Limited Report, AECL-11831, COG-97-319-I.

King, F., L. Ahonen, C. Taxén, U. Vuorinen and L. Werme. 2001. Copper corrosion under expected conditions in a deep geologic repository. Swedish Nuclear Fuel and Waste Management Company Report, SKB TR 01-23.

King, F., M. Kolar and S. Stroes-Gascoyne. 2002a. Theory manual for the microbiological copper corrosion model CCM-MIC.0. Ontario Power Generation, Nuclear Waste Management Division Report 06819-REP-01200-10091-R00. Toronto, Ontario.

King, F., L. Ahonen, C. Taxén, U. Vuorinen, and L. Werme. 2002b. Copper corrosion under expected conditions in a deep geologic repository. Posiva Oy Report POSIVA 2002-01.

King, F., M. Kolar, and S. Stroes-Gascoyne. 2003. Preliminary simulations of the long-term activity of microbes in a deep geologic repository using CCM-MIC.0 and the implications for corrosion of copper containers. Ontario Power Generation Nuclear Waste Management Division Report No: 06819-REP-01200-10116.

King, F., M. Kolar, S. Stroes-Gascoyne, and P. Maak. 2004. Model for the microbiological corrosion of copper containers in a deep geologic repository. In Scientific Basis for Nuclear Waste Management XXVII, (V.M. Oversby and L.O. Werme, Editors), Mat. Res. Soc. Symp. Proc. 807, Materials Research Society, (Warrendale, PA), 811-816.

Kolar, M. 2006. TRANSIENT - A C package for the numerical solution of systems of partial differential equations of parabolic type. http://transient.mkolar.org/.

Kolar, M. and F. King. 1996. Modelling the consumption of oxygen by container corrosion and reaction with Fe(II)," Mats. Res. Soc. Symp. Proc. 412, Materials Research Society, Pittsburgh, PA, 547-554.

Lee, H.P. and K. Nobe. 1986. Kinetics and mechanisms of Cu electrodissolution in chloride media. Journal Electrochemical Society 133, 2035-2043.

Lee, H.P., K. Nobe and A.J. Pearlstein. 1985. Film formation and current oscillations in the electrodissolution of Cu in acidic chloride media. I. Experimental studies. Journal Electrochemical Society 132, 1031-1037.

Lee, S. and R.W. Staehle. 1997. Adsorption of water on copper, nickel, and iron. Corrosion 53, 33-42.

Leygraf, C. and T.E. Graedel. 2000. Atmospheric Corrosion. Wiley-Interscience, New York.

Litke, C.D., S.R. Ryan and F. King. 1992. A mechanistic study of the uniform corrosion of copper in compacted clay-sand soil, Atomic Energy of Canada Limited Report, AECL-10397, COG-91-304.

Maak, P. 1999. The selection of a corrosion-barrier primary material for used-fuel disposal containers. Ontario Power Generation, Nuclear Waste Management Division Report 06819-REP-01200-10020-R00.

Maak, P. 2006. Used fuel container requirements. Ontario Power Generation Preliminary Design Requirements. 06819-PDR-01110-10000 R02.

Masurat, P., S. Eriksson, and K. Pedersen. 2007. Microbial sulphide production in compacted Wyoming MX-80 bentonite under *in situ* conditions relevant to a repository for high level radioactive waste. In Proceedings of the Workshop on Long-term Performance of Smectitic Clays Embedding Canisters with Highly Radioactive Waste, Lund, Nov. 26-28, 2007.

Matlosz, M. and J. Newman. 1987. Solving 1-D boundary-value problems with BandAid: A functional programming style and a complementary software tool. Computer Chemical Engineering 11, 45-61.

Mazurek, M. 2004. Long-term used nuclear fuel waste management – geoscientific review of the sedimentary sequence in southern Ontario. Nuclear Waste Management Office Background Paper 6-12.

McMurray, J. 2004. Reference water compositions for a deep geologic repository in the Canadian Shield. Ontario Power Generation, Nuclear Waste Management Division Report 06819-REP-01200-10135-R01.

McMurray, J., D.A. Dixon, J.D. Garroni, B.M. Ikeda, S. Stroes-Gascoyne, P. Baumgartner, and T.W. Melnyk. 2003. Evolution of a Canadian deep geologic repository: base scenario. Ontario Power Generation, Nuclear Waste Management Division Report 06819-REP-01200-10092-R00.

Moreau, A. 1981a. Etude du mecanisme d'oxydo-reduction du cuivre dans les solutions chlorurees acides-I. Systeme Cu-. Electrochimica Acta 26, 497-504.

Moreau, A. 1981b. Etude du mecanisme d'oxydo-reduction du cuivre dans les solutions chlorurees acides-II. Systemes Cu-CuCl- et Cu-$Cu_2(OH)_3Cl$-$CuCl^+Cu^{2+}$. Electrochimica Acta 26, 1609-1616.

Moreau, A., J.P. Frayret, F. Del Rey and R. Pointeau. 1982. Etude des phenomenes electrochimiques et des transports de matiere d'un systeme metal electrolytique: Cas d'un disque tournant en cuivre dans des solutions aqueuses d'acide chlorhydrique. Electrochimica Acta 27, 1281-1291.

Nagano, H., T. Doi, and M. Yamashita. 1998. Study on water adsorption-desorption on metal surfaces and the early stage of atmospheric corrosion in steels. Materials Science Forum 289-292, 127-134.

Nagra. 2002. Project Opalinus Clay. Safety Report. Nagra Technical Report 02-05.

Newman, J. 1973. Electrochemical Systems. Prentice-Hall, Englewood Cliffs, NJ.

Nguyen, T.V. and R.E. White. 1987. A finite difference procedure for solving coupled nonlinear, elliptic partial differential equations. Computer Chemical Engineering 11, 543-546.

NWMO. 2005. Choosing a way forward. The future management of Canada's used nuclear fuel. Final study. Nuclear Waste Management Organization, Toronto, Ontario.

Pedersen K. 2000. Microbial processes in radioactive waste disposal. Swedish Nuclear Fuel and Waste Management Company Report, SKB TR 00-04.

Peters, D.G. and S.A. Cruser. 1965. Cathodic chronopotentiometry of copper(I) and copper(II) in chloride media. Journal Electroanalysis Chemistry 9, 27-40.

Russell, S.B. and G.R. Simmons. 2003. Engineered barrier system for a deep geological repository in Canada. In Proc. 10th Int. High-Level Radioactive Waste Management Conf., Las Vegas, NV, March 30-April 2, 2003 (American Nuclear Society, La Grange Park, IL), pp. 563-570.

Ryan, S.R. and F. King. 1994. The adsorption of Cu(II) on sodium bentonite in a synthetic saline groundwater. Atomic Energy of Canada Limited Report, AECL-11062, COG-I-94-125.

Sharma, V.K. and F.J. Millero. 1988. The oxidation of Cu(I) in electrolyte solutions. Journal Solution Chemistry 17, 581-599.

Sharma, V.K. and F.J. Millero. 1990. Equilibrium constants for the formation of Cu(I) halide complexes. J. Solution Chem. 19, 375-390.

Shoesmith, D.W. and F. King. 1999. The effects of gamma radiation on the corrosion of candidate materials for the fabrication of nuclear waste packages. Atomic Energy of Canada Limited Report, AECL-11999.

Shreir, L.L. 1976. Corrosion. 2nd edition, Newnes-Butterworths, London.

Smyrl, W.H. 1985. Digital impedance for Faradaic analysis. II. Electrodissolution of Cu in HCl. Journal Electrochemical Society 132, 1555-1562.

Spiessl, S.M., K.U. Mayer and K.T.B. MacQuarrie. 2006. Reactive transport modelling in fractured rock – rock stability study. Ontario Power Generation, Nuclear Waste Management Division Report 06819-REP-01200-10160.

Spotnitz, R. 1994. NL3BAND. Technical Software Distributors. Charlotte, NC.

Stroes-Gascoyne, S., C.J. Hamon, C. Kohle, and D.A. Dixon. 2006. The effects of dry density and porewater salinity on the physical and microbiological characteristics of highly compacted bentonite. Ontario Power Generation, Nuclear Waste Management Division Report 06819-REP-01200-10016.

Stroes-Gascoyne, S., C.J. Hamon, D.A. Dixon, C. Kohle, and P. Maak. 2007. The effects of dry density and porewater salinity on the physical and microbiological characteristics of highly compacted bentonite. In Scientific Basis for Nuclear Waste Management XXX, edited by Darrell Dunn, Christophe Poinssot, Bruce Begg (Mater. Res. Soc. Symp. Proc. 985, Warrendale, PA, 2007), paper 0985-NN13-02.

Stumm, W. 1992. Chemistry of the Solid-Water Interface: Processes at the Mineral-Water and Particle-Water Interface in Natural Systems, Wiley-Interscience (New York, NY).

Vazquez, M.V., S.R. de Sanchez, E.J. Calvo and D.J. Schiffrin. 1994a. The electrochemical reduction of oxygen on polycrystalline copper in borax buffer. Journal Electroanalysis Chemistry 374, 189-197.

Vazquez, M.V., S.R. de Sanchez, E.J. Calvo and D.J. Schiffrin. 1994b. The electrochemical reduction of hydrogen peroxide on polycrystalline copper in borax buffer. Journal Electroanalysis Chemistry 374, 179-187.

White, R.E. 1978. On Newman's numerical technique for solving boundary value problems. Industrial Engineering Chemical Fundamentals 17, 367-369.

APPENDIX A: INPUT DATA FOR CCM-UC.1.1

CONTENTS

APPENDIX A: INPUT DATA FOR CCM-UC.1.1

The input parameters are grouped under the following headings: Control Parameters, Layer-dependent Parameters and Material, Rate and Environment Parameters. Control parameters determine, amongst other things, the speed and accuracy of the computer code; grid parameters define the spatial grid; and material, rate and environment parameters describe the various mass-transport, chemical and electrochemical processes.

A.1 CONTROL PARAMETERS

The following are the control parameters for the subroutine TRANSIENT (Kolar 2006) and are common to all programs that include this subroutine, including the current model.

monitor — Level of diagnostic output (monitor = 2). Four settings of monitor between 0 and 3 determine the amount of information displayed on-screen during the execution.

steady — Designates type of solution (steady = 0). The code can calculate either a transient (steady = 0), a steady-state solution (steady = 1), or calculate the steady-state solution and then use it as input for the transient solution (steady = 2).

tau — The degree of implicitness for the differencing scheme (tau = 0.5). Tau = 0 corresponds to a fully implicit solution, 0.5 to a Crank-Nicholson solution and 1 to an explicit solution. Generally, the Crank-Nicholson solution is used.

CTOL — Relative c tolerance for the Newton-Raphson (NR) iterations. The NR iterations are assumed to converge when the relative change in $\underset{\max}{\Delta c(l)}$ (Equation (931)) is less than CTOL and when the absolute value of $F_k^{(j)}$ (Equation (82a)) is less than $FTOL \cdot \sqrt{|tStep|}$, where tStep is the length of the time step. See next parameter.

FTOL — $FTOL \cdot \sqrt{|tStep|}$ is the absolute F tolerance for the NR iteration. See previous parameter.

nIter — Desired number of NR iterations in each time step (5).

iterMax — Maximum number of NR iterations in each time step.

tStart — Initial time in s (0 s). Start of integration.

tEnd — Final time in s (variable). End of integration.

tStepMax — The largest time step allowed in s (-1 s). For tStepMax $\leq$ 0, there is no limitation on the time step.

attemptMax — Maximum number of attempts at choosing next time step (30).

strict — Parameter determining extent to which cDiffMax is used to calculate the next time step (-1, 0,1). Using strict < 0, cDiffMax is not used at all in determining the next time step; strict = 0, cDiffMax is not exceeded too much; strict > 0, cDiffMax is strictly enforced (within 18%). In general, the higher the value of strict, the more accurate, but slower, the code execution.

tOutInit — Initial output time tOut in s for the concentration profiles (variable).

tOutMulF — Multiplication factor to determine the next value of tOut (1.5). Thus, $tOut_{n+1} = tOut_n + tOut_{n-1}tOutMulF$.

nOutOTH — Number of profiles calculated between consecutive tOut values (20).

sepProf — Parameter determining how output files are stored (1). For sepProf = 0, all output files are stored in a single file; for sepProf = 1, profiles for each time output are stored in a separate file.

init_from_file — Name of file containing initial profiles. Used when profiles other than determined by initial concentrations are to be used as the input data. Useful for re-starting stalled runs.

A.2 LAYER-DEPENDENT PARAMETERS

Nmedia — Number of layers in the model.

mediumNo — Number designation of the layer.

NMlayer — Name given to the layer, e.g., inner buffer, outer buffer, EDZ, etc.

L — Thickness of layer.

dx — Thickness of first grid spacing of layer.

epsE — Effective (or through) porosity for mass transport.

epsS — Storage porosity

epsN — Non-accessible porosity

rho — Dry density

S_{MIC} — Degree of saturation below which microbial activity does not occur, based on a threshold water activity of 0.96.

c_5^{max} — Maximum adsorption capacity of layer for Cu^{2+}.

A_F — Specific surface area of Fe(II) minerals.

τ_f — Tortuosity factor.

k_9 First order rate constant for the consumption of O_2 by aerobic bacteria.

c_A Initial concentration of gaseous O_2.

c_0 Initial concentration of dissolved O_2.

c_6 Initial Cl^- ion concentration.

c_7 Initial dissolved Fe(II) concentration.

S(t) Time-dependent degree of saturation for the layer.

K(S) Saturation-dependent thermal conductivity.

C_p Specific heat.

A.3 MATERIAL, RATE, AND ENVIRONMENTAL PARAMETERS

k_1 Rate constant for the homogeneous oxidation of $CuCl_2^-$ by O_2 (a function of T and $[Cl^-]$ according to Equation (55b) and calculated within the model, rather than being inputted as a distinct input parameter). The temperature dependence is taken directly from Sharma and Millero (1988), and is equivalent to an activation energy of 39.5 $kJ \cdot mol^{-1}$. This value was used by these authors for pure NaCl solutions in the pH range 6-9 and for Cl^- solutions with additions of HCO_3^- and Mg^{2+} (or Ca^{2+}), and is valid over the temperature range 5-45°C. For seawater, they used an activation energy of 45.4 $kJ \cdot mol^{-1}$, valid over the same pH and T ranges.

A problem arises, however, with the application of their data to Na/Ca chloride mixtures. Experimentally, Mg^{2+} was found to decrease the rate of Cu(I) oxidation, it was thought by competing with Cu^{2+} for complexation with the EDTA added to the solution (taken to be equivalent to the effect of Na-bentonite in our system). Although only studied over a limited concentration range, Ca^{2+} was said to have the same effect as Mg^{2+}, and the combined concentration could be used in the quoted polynomial expressions for k_1. However, the use of these expressions at high $[CaCl_2]$, as might be formed from concentrated fluids, leads to anomalous results. Sharma and Millero's polynomial expressions are obviously invalid at high $[Ca^{2+}+Mg^{2+}]$, because k_1 is larger in Ca/Mg brines than in pure NaCl of the same $[Cl^-]$. Similarly, the polynomial for seawater, which might be a better analogue for Ca brines than pure NaCl, gives decreasing k_1 up to an ionic strength of 1 $mol \cdot dm^{-3}$, but increasing k_1 at higher ionic strengths. Given these anomalies, we have taken the expression for pure NaCl solutions for k_1 ($[Cl^-]$, T, pH), which may underestimate the effect of Ca^{2+} on k_1. The derived expression (Equation (55b)) is for a constant pH of 7.

k_2 Rate constant for the hydrolysis of $CuCl_2^-$ (1 s^{-1} at 25°C). The mechanism for the formation of Cu_2O is unknown, but is assumed here to result from the hydrolysis

of $CuCl_2^-$. The value of k_2 is set a factor of 10 larger than k_{-2} in order to simulate the experimentally observed formation of Cu_2O.

ΔH_2 Temperature dependence of k_2 (60 $kJ \cdot mol^{-1}$). Estimated value based on a typical ΔH for chemical processes.

k_{-2} Rate constant for the dissolution of Cu_2O (0.1 s^{-1} at 25°C). Some experimental data are available on the dissolution rate of Cu_2O in Cl^- solutions as a function of pH (King and Legere, unpublished data), including an activation energy, the dependence on pH and $[Cl^-]$ and estimated values for the rate constant in units of $mol \cdot cm^{-2} \cdot s^{-1}$. The reaction is pH-dependent, but independent of $[Cl^-]$. However, k_{-2} is expressed in terms of the rate of Cu_2O dissolution per unit volume. Consequently, a value for the specific surface area of Cu_2O ($cm^2 \cdot mol^{-1}$) is required to convert the experimentally accessible rate constant to k_{-2}. The specific surface area of Cu_2O is unknown and will depend on the environmental conditions under which precipitation occurs. Therefore, the value of k_{-2} of 0.1 s^{-1} is an assumed value.

ΔH_{-2} Temperature dependence of k_{-2} (40 $kJ \cdot mol^{-1}$). Based on experimental data on Cu_2O dissolution at pH 5 (King and Legere, unpublished data).

k_3 Rate constant for the precipitation of $CuCl_2 \cdot 3Cu(OH)_2$ (1 x $10^{-5} \cdot s^{-1}$ at 25°C). There are no kinetic data for the rate of precipitation of $CuCl_2 \cdot 3Cu(OH)_2$. The precipitation rate constant is 10 times higher than the dissolution rate constant to account for the experimental observation of precipitated $CuCl_2 \cdot 3Cu(OH)_2$. The value of k_3 of 1 x 10^{-5} s^{-1} is assumed.

ΔH_3 Temperature dependence of k_3 (60 $kJ \cdot mol^{-1}$). Estimated value based on a typical ΔH for chemical processes.

k_{-3} Rate constant for the dissolution of $CuCl_2 \cdot 3Cu(OH)_2$ (1 x 10^{-6} s^{-1} at 25°C). There are a limited number of measurements on the dissolution rate of $CuCl_2 \cdot 3Cu(OH)_2$ (King and Strandlund, unpublished data). However, as in the case of the dissolution of Cu_2O (k_{-2}), k_{-3} contains a term for the specific surface area of precipitated $CuCl_2 \cdot 3Cu(OH)_2$, an unknown parameter. Therefore, an assumed value of k_{-3} is used.

ΔH_{-3} Temperature dependence of k_{-3} (60 $kJ \cdot mol^{-1}$). Estimated value based on a typical ΔH for chemical processes.

k_4 Rate constant for the adsorption of Cu^{2+} on Na-bentonite (2 x 10^{-3} $dm^3 \cdot mol^{-1} \cdot s^{-1}$ at 25°C). The rate of Cu^{2+} adsorption is based on unpublished data (King and Ryan) from studies on loose clay. The form of the kinetic adsorption expression is consistent with the nature of the equilibrium Langmuir isotherm observed experimentally (Ryan and King 1994).

ΔH_4 Temperature dependence of k_4 (0 $kJ \cdot mol^{-1}$). Various equilibrium sorption studies of Cu^{2+} on loose montmorillonite clay report both positive and negative enthalpies (Ryan and King 1994). Therefore, in the absence of other data, the adsorption of Cu^{2+} will be assumed to be independent of temperature.

k_{-4} Rate constant for the desorption of Cu^{2+} (1×10^{-6} s^{-1} at 25°C). The desorption rate constant is an estimated value based on the observation of extremely slow desorption in loose clay systems (King and Ryan, unpublished data).

ΔH_{-4} Temperature dependence of k_{-4} (0 $kJ \cdot mol^{-1}$). Various equilibrium sorption studies of Cu^{2+} on loose montmorillonite clay report both positive and negative enthalpies (Ryan and King 1994). Therefore, in the absence of other data, the desorption of Cu^{2+} will be assumed to be independent of temperature.

k_5 Rate constant for the reaction between O_2 and dissolved Fe(II) (2.9 $dm^3 \cdot mol^{-1} \cdot s^{-1}$ at 25°C). This reaction is highly pH dependent. The value is derived from the estimated pseudo-first-order (with respect to [Fe(II)]) rate constant in oxygenated solution at pH 7, 3.7×10^{-3} s^{-1} (Wehrli 1990). This corresponds to a value of k_5 of 2.9 $dm^3 \cdot mol^{-1} \cdot s^{-1}$ for an $[O_2]$ of 1.26×10^{-3} $mol \cdot dm^{-3}$, on the assumption that the reaction is first order with respect to $[O_2]$. Wehrli (1990) does not quote a temperature, which is assumed to be 25°C.

ΔH_5 Temperature dependence of k_5 (40 $kJ \cdot mol^{-1}$). Activation energy assumed to be the same as that for k_1.

k_6 Rate constant for the reaction between Cu^{2+} and Fe(II) (10 $dm^3 \cdot mol^{-1} \cdot s^{-1}$ at 25°C). No experimental data are available. The value is based on the assumption that the homogeneous kinetics are rapid, as is the case for the redox reactions involving O_2 and $CuCl_2^-$ and O_2 and Fe(II) discussed above.

ΔH_6 Temperature dependence of k_6 (40 $kJ \cdot mol^{-1}$). Activation energy assumed to be the same as that for k_1.

R_0 Instantaneous dissolution rate (expressed as the Fe(II) release rate) of the Fe(II) mineral phase at 25°C. The model used for predicting the release rate of Fe(II) from dissolution of the Fe(II) mineral phase is based on the experimental observation that an Fe(II)-depleted layer of constant thickness forms on the dissolving surface. During the transient period, the thickness of this layer grows. At steady-state (i.e., once a constant film thickness has been achieved), the dissolution rate of the film (and, hence, the release rate of Fe(II)) is determined by the dissolution rate of the least soluble component. In general, the values of R_0, R_1 and α_F can be used to describe the dissolution rate of any Fe(II)-containing solid.

ΔH_{R_O} Temperature dependence of R_0.

R_1 Steady-state dissolution rate of the Fe(II) mineral phase.

ΔH_{R_1} Temperature dependence of R_1.

α_F Time constant for the dissolution of the Fe(II) mineral phase.

ΔH_{α_F} Temperature dependence of α_F.

k_7 Rate constant for the rate of precipitation of an unidentified Fe(II) solid (1.0 s^{-1} at 25°C). Rate constants k_7 and k_{-7} are included in the model to simulate the precipitation and subsequent re-dissolution of a secondary Fe(II) solid phase. This phase forms if the rate of dissolution of Fe(II) from the initially present Fe(II) phase exceeds the rate at which it is consumed in redox reactions with either O_2 or Cu^{2+}. Under these conditions, Fe(II) will accumulate in the system and could eventually exceed the solubility of a secondary Fe(II) solid. These processes simulate the transformation of the original Fe(II) phase to a more stable Fe(II) solid. In the absence of experimental evidence for this process, k_7 is assumed to have the same value as that for the precipitation of Cu_2O.

ΔH_7 Temperature dependence of k_7 (60 kJ·mol^{-1}). Estimated value based on a typical ΔH for chemical processes.

k_{-7} Rate constant for the dissolution of a Fe(II) secondary phase (0.1 s^{-1} at 25°C). See comments above for k_7. Value of k_{-7} assumed to be the same as that for the dissolution rate of Cu_2O.

ΔH_{-7} Temperature dependence of k_{-7} (60 kJ·mol^{-1}). Estimated value based on a typical ΔH for chemical processes.

k_8 Rate constant for the dissolution of gaseous O_2 (0.0122 s^{-1} at 25°C).

ΔH_8 Temperature dependence of k_8 (60 kJ·mol^{-1}).

ΔH_9 Temperature dependence of k_9 (60 kJ·mol^{-1}).

D_A Diffusion coefficient of gaseous O_2 in air (0.00165 $dm^2 \cdot s^{-1}$ at 25°C).

ΔH_{D_A} Temperature dependence of D_A (-2.06 kJ·mol^{-1} at 25°C), based on the temperature dependence of the viscosity of air.

D_0 Pore-solution diffusion coefficient of O_2 (1.7 x 10^{-7} $dm^2 \cdot s^{-1}$ at 25°C). From data of King et al. (1995a).

ΔH_{D_O} Temperature dependence of D_0 (15 kJ·mol^{-1}). In the absence of other data, the activation energy for the diffusion of dissolved species is taken to be the same as that for the temperature dependence of the viscosity of H_2O.

D_1 Pore-solution diffusion coefficient of $CuCl_2^-$ (6 x 10^{-8} $dm^2 \cdot s^{-1}$ at 25°C). From data of Smyrl (1985).

ΔH_{D1} Temperature dependence of D_1 (18.8 kJ·mol^{-1}). From Bacarella and Griess (1973).

D_3 Pore-solution diffusion coefficient of Cu^{2+} (6 x 10^{-8} $dm^2 \cdot s^{-1}$ at 25°C). From data of Miller et al. (1980) in $CuSO_4$ solutions and Peters and Cruser (1965) in Cl^- solution.

ΔH_{D_3} Temperature dependence of D_3 (15 kJ·mol^{-1}). In the absence of other data, the activation energy for the diffusion of dissolved species is taken to be the same as that for the temperature dependence of the viscosity of H_2O.

D_6 Pore-solution diffusion coefficient of Cl^- (2 x 10^{-7} cm^2·s^{-1} at 25°C). From Fontana et al. (1985).

ΔH_{D_6} Temperature dependence of D_6 (15 kJ·mol^{-1}). In the absence of other data, the activation energy for the diffusion of dissolved species is taken to be the same as that for the temperature dependence of the viscosity of H_2O.

f_{D_6} Enhancement factor to account for the effect of gravitational mixing of saline rock-mass fluids (variable).

D_7 Pore-solution diffusion coefficient of Fe(II) (5 x 10^{-8} dm^2·s^{-1} at 25°C). From International Critical Tables (ICT 1926).

ΔH_{D7} Temperature dependence of D_7 (15 kJ·mol^{-1}). In the absence of other data, the activation energy for the diffusion of dissolved species is taken to be the same as that for the temperature dependence of the viscosity of H_2O.

c_1^{sat} Concentration of $CuCl_2^-$ in equilibrium with Cu_2O (3.4 x 10^{-3} mol·dm^{-3} at 25°C in 1 mol·dm^{-3} Cl^-, pH 7). The concentration of $CuCl_2^-$ in equilibrium with Cu_2O is equated to the total concentration of dissolved Cu(I) species (Cu^+, $CuCl_2^-$, Cu(OH) and $Cu(OH)_2^-$. No Cu(II) species are included in the equilibrium calculations. The solubility of Cu_2O is a function of $[Cl^-]$ and temperature (see Equation (60) in the main text). Since, in the pH and $[Cl^-]$ ranges of interest (King and Kolar 2000), $CuCl_2^-$ is the dominant species, the solubility of Cu_2O is proportional to $[Cl^-]^2$. The pH is assumed to be constant in the model.

ΔH_1^{sat} Temperature dependence of c_Δ^{sat} (24 kJ·mol^{-1}). Determined from the effect of temperature on the solubility of Cu_2O (D.J. Jobe, private communication).

c_3^{sat} Concentration of Cu^{2+} in equilibrium with $CuCl_2·3Cu(OH)_2$ (4.3 x 10^{-7} mol·dm^{-3} at 25°C, pH 7). The concentration of Cu^{2+} in equilibrium with $CuCl_2·3Cu(OH)_2$ is equated to the sum of the concentrations of all major dissolved species, namely; Cu^{2+}, $Cu(OH)^+$, $Cu(OH)_2$, $Cu(OH)_4^{2-}$ and $CuCl^+$ (D.J. Jobe, private communication). No Cu(I) species are considered in the equilibrium calculations. The relative proportions of these various species is a function of T, $[Cl^-]$ and pH. At $[Cl^-]$ < 0.1 mol·dm^{-3}, the solubility of $CuCl_2·3Cu(OH)_2$ is proportional to $[Cl^-]^{-0.5}$, as would be expected from the stoichiometry. At higher $[Cl^-]$ (0.1 < $[Cl^-]$ <1.0 mol·dm^{-3}), the solubility is approximately independent of $[Cl^-]$. Therefore, c_3^{sat} is assumed to be independent of $[Cl^-]$ for the present calculations.

ΔH_3^{sat} Temperature dependence of c_3^{sat} (19 kJ·mol^{-1}). The temperature dependence of c_3^{sat} varies with temperature. The value quoted is a mean of several values determined between 25°C and 100°C (D.J. Jobe, private communication).

c_7^{sat} Concentration of dissolved Fe(II) in equilibrium with a precipitated Fe(II) secondary phase (1×10^{-5} mol·dm^{-3} at 25°C). Malmstrom et al. (1995) cited an observed [Fe(II)] in a fracture of 1×10^{-5} mol·dm^{-3}, which will be used here in the absence of other data.

$\Delta H_7^{sat\ t}$ Temperature dependence of c_7^{sat} (30 kJ·mol^{-1}). An assumed value.

Farad Faraday constant (96 487 C·mol^{-1}).

R Gas constant (8.314 J·K^{-1}·mol^{-1}).

n_0 Number of electrons transferred in the reduction of O_2 (4). From King et al. (1995a).

α_{c1} Cathodic transfer coefficient for the reduction of O_2 (0.37). The transfer coefficient is a function of [O_2] (King et al. 1995b). The value used is that for aerated solution.

k_c Electrochemical rate constant for the reduction of O_2 (1.7×10^{-9} dm·s^{-1} at 25°C). From King et al. (1995a).

ΔH_c Temperature dependence of k_c (60 kJ·mol^{-1}). From Kinoshita (1992).

E_c^0 Standard potential for Reaction (4) in the main text (0.16 V_{SCE} at 25°C). E_c^0 is corrected to pH 7, so that the exponential term in the expression for the equilibrium potential of Reaction (4) is not pH-dependent.

ΔE_c^0 Temperature dependence of E_c^0 (-1.23×10^{-4} V·K^{-1}). Calculated on the assumption of a linear temperature dependence of E_c^0 between 298.2 K and 368.2 K. The values of E_c^0 at these temperatures was calculated using the convention that the free energy of the standard hydrogen electrode (SHE) is zero only at 298.2 K. Therefore, the standard potential of the SHE changes with temperature.

n_a Number of electrons transferred during the oxidation of Cu (1). From King et al. (1995a).

E_a^0 Standard potential for Reaction (1) in the main text (-0.105 V_{SCE} at 25°C). From King et al. (1995a).

ΔE_a^0 Temperature dependence of E_a^0 (-6.35×10^{-4} V·K^{-1}). From Bertocci and Turner (1974).

k_a Combined electrochemical rate constant for the anodic dissolution of Cu (3.3×10^{-4} dm·s^{-1} at 25°C). k_a is a combined rate constant, equivalent to $k_{af}k_{bf}/k_{ab}$ (see Reactions (1) and (2) in the main text). The value of k_a is a mean value from 0.1 mol·dm^{-3} and 1.0 mol·dm^{-3} Cl^- solution (King et al. 1995a).

ΔH_a Temperature dependence of k_a (60 kJ·mol^{-1}). Assumed value.

k_{bb}	Rate constant for the reverse of Reaction (2) in the main text (1.42×10^{-3} dm·s^{-1} at 25°C). From King et al. (1995a).
ΔH_{bb}	Temperature dependence of k_{bb} (60 kJ·mol^{-1}). Assumed value.
n_2	Number of electrons transferred for the reduction of Cu^{2+} (1).
k_d	Electrochemical rate constant for the reduction of Cu^{2+} (2×10^{-8} dm·s^{-1} at 25°C). Value derived from i/E curves of Hurlen (1961).
ΔH_d	Temperature dependence of k_d (45 kJ·mol^{-1}). From Astakhova and Krasikov (1971).
α_d	Transfer coefficient for the reduction of Cu^{2+} (0.5). Assumed value based on facile electron transfer reaction.
E_d^0	Standard potential for Reaction (5) in the main text (0.223 V_{SCE} at 25°C). From Van Muylder et al. (1961) and Peters and Cruser (1965).
ΔE_d^0	Temperature dependence of E_d^0 (0 V·K^{-1}). Temperature dependence unknown.
T_{room}	Ambient temperature (298.15 K).
$T_{container}(t)$	Time-dependent temperature at the container surface.
$T_{right}(t)$	Time-dependent temperature at the right-hand boundary.
$T_{initital}(x)$	Initial spatially dependent repository temperature.
c_{0R}	Concentration of dissolved O_2 at the right-hand boundary.
c_{6R}	Concentration of Cl^- ions at the right-hand boundary.
rhoW	Density of water (1.0204 kg·dm^{-3}).
h_k	Time-dependent humidity at the container surface.
h_k^{min}	Minimum threshold humidity for electrochemical reactions (0.6).
h_k^{max}	Maximum threshold humidity for electrochemical reactions (0.7).

REFERENCES FOR APPENDIX A

Astakhova, R.K. and B.S. Krasikov. 1971. Electrochemical behaviour of copper in chloride electrolytes. Applied Chemistry USSR 44, 356-362.

Bacarella, A.L. and J.C. Griess Jr. 1973. The anodic dissolution of copper in flowing sodium chlroide solutions from 25°C and 175°C. Electrochemical Society 120, 459-465.

Bertocci, U. and D.R. Turner. 1974. Copper. In Encyclopedia of the Electrochemistry of the Elements, (Editor, A.J. Bard), Volume II. Marcel Dekker, New York, NY, Ch. II-6, Table 1.1.2.

Fontana, A., J. Van Muylder and R. Winand. 1985. Etablissement de diagrammes tension-pH cinetiques du cuivre en milieu de chlorures. Electrochimica Acta 30, 641-647.

Hurlen, T. 1961. Dissolution of copper by oxidation agents in acid chloride solution. Acta Chem. Scand. 15, 1239-1245.

ICT. 1926. International Critical Tables of Numerical Data, McGraw-Hill, New York, NY.

King, F. and M. Kolar. 2000. The copper container corrosion model used in AECL's second case study. Ontario Power Generation, Nuclear Waste Management Division Report 06819-REP-01200-10041-R00. Toronto, Ontario.

King, F., C.D. Litke, M.J. Quinn and D.M. LeNeveu. 1995a. The measurement and prediction of the corrosion potential of copper in chloride solutions as a function of oxygen concentration and mass-transfer coefficient. Corrosion Science 37, 833-851.

King, F., M.J. Quinn and C.D. Litke. 1995b. Oxygen reduction on copper in neutral NaCl solution. Electroanalysis Chemistry 385, 45-55.

Kinoshita, K. 1992. Electrochemical Oxygen Technology. Wiley, New York, NY, Table 2.3.

Kolar, M. 2006. TRANSIENT - A C package for the numerical solution of systems of partial differential equations of parabolic type. http://transient.mkolar.org/.

Malmström, M., S. Banwart, L. Duro, P. Wersin and J. Bruno. 1995. Biotite and chlorite weathering at 25°C. Swedish Nuclear Fuel and Waste Management Company Technical Report, TR 95-01.

Miller, D.G., J.A. Rard, L.B. Eppstein and R.A. Robinson. 1980. Mutual diffusion coefficients, electrical conductances, osmotic coefficients, and ionic transport coefficients l_{ij} for aqueous $CuSO_4$ at 25°C. Solution. Chem. 9, 467-496.

Peters, D.G. and S.A. Cruser. 1965. Cathodic chronopotentiometry of copper(I) and copper(II) in chloride media. Electrochemical Society 9, 27-40.

Ryan, S.R. and F. King. 1994. The adsorption of Cu(II) on sodium bentonite in a synthetic saline groundwater. Atomic Energy of Canada Limited Report, AECL-11062, COG-I-94-125.

Sharma, V.K. and F.J. Millero. 1988. The oxidation of Cu(I) in electrolyte solutions. Solution Chemistry 17, 581-599.

Smyrl, W.H. 1985. Digital impedance for Faradaic analysis. Part II. Electrodissolution of Cu in HCl. Electrochemical Society 132, 1555-1562.

Van Muylder, J., N. de Zoubov and M. Pourbaix. 1961. Diagrammes d'equilibres tension-pH des systemes Cu-H_2O et Cu-Cl^--H_2O a 25^{o}C. CEBELCOR Report (Centre Belges D'Etudes de la Corrosion, Brussels), Report No. 755.

Wehrli, B. 1990. Redox reactions of metal ions at mineral surfaces. In Aquatic Chemical Kinetics, (Editor, W. Stumm), Wiley-Interscience, New York, NY, Chapter 11.